NASA Contractor Report 182091
ICASE Report No. 90–58

ICASE

SECONDARY INSTABILITIES IN COMPRESSIBLE BOUNDARY LAYERS

Lian Ng
G. Erlebacher

Contract No. NAS1–18605
September 1990

Institute for Computer Applications in Science and Engineering
NASA Langley Research Center
Hampton, Virginia 23665–5225

Operated by the Universities Space Research Association

National Aeronautics and
Space Administration

Langley Research Center
Hampton, Virginia 23665-5225

(NASA-CR-182091) SECONDARY INSTABILITIES IN COMPRESSIBLE BOUNDARY LAYERS Final Report (NASA) 52 p CSCL 01A
N90-28592
Unclas
G3/02 0305025

Secondary Instabilities in Compressible Boundary Layers

Lian Ng

NASA Langley Research Center

G. Erlebacher

Institute for Computer Applications in Science and Engineering

ABSTRACT

This paper examines (linear) secondary instabilities in compressible boundary layers at Mach numbers $M_\infty = 0, 0.8, 1.6$ and 4.5. We find that there is a broad-band of highly unstable 3-d secondary disturbances whose growth rates increase with increasing primary wave amplitude. At $M_\infty \leq 1.6$, fundamental resonance dominates at relatively high (2-d) primary disturbance amplitude, while subharmonic resonance is characterized by a low (2-d) primary amplitude. At $M_\infty = 4.5$, the subharmonic instability which arises from the second mode disturbance is the strongest type of secondary instability.

The influence of the inclination, θ, of the primary wave with respect to the mean flow direction on secondary instability is investigated at $M_\infty = 1.6$ for small to moderate values of θ. It is found that the strongest fundamental instability occurs when the primary wave is inclined at 10° to the mean flow direction, although a 2-d primary mode yields the most amplified subharmonic. The subharmonic instability at a high value of θ (namely, $\theta = 45^0$) is also discussed.

Finally, a subset of the secondary instability results are compared against direct numerical simulations.

* Research supported by the National Aeronautics and Space Administration under contract No. NAS1-18605 while resident at the Institute for Computer Applications in Science and Engineering (ICASE), NASA Langley Research Center, Hampton, VA 23665.

I. Introduction

In view of the renewed interest in high speed technology such as the National Aero-Space Plane project, a good understanding of boundary-layer transition in supersonic and hypersonic flows is crucial to the design of efficient aerodynamic vehicles. For example, an accurate estimate of aerodynamic drag and surface heating for supersonic aircraft requires a good knowledge of transition physics.

Although little is known, either experimentally or theoretically, on the paths to transition in compressible boundary layers, it is well known that the early stages of transition in incompressible boundary layers often occur via (i) primary and (ii) secondary instability mechanisms. Typically, when the amplitude of the primary wave (or interchangeably, TS wave) becomes sufficiently large (as it propagates downstream), the flow becomes very unstable to three-dimensional (3-d) secondary disturbances. These 3-d disturbances are responsible for three known laminar-turbulent transition routes. The first is the fundamental (K) type breakdown in which the lambda-shaped vortices are aligned along their peaks in the streamwise direction, repeating every TS wavelength. The second is called the subharmonic (H) type breakdown: the lambda vortices are staggered, repeating at a streamwise distance equal to twice the TS wavelength. The third type of breakdown is called detuned: the spacing of the lambda vortices lies between that of the K type and the H type. The K type breakdown often occurs at a higher TS amplitude than does the H-type. Herbert et. al. [7] have shown that the paths to these breakdowns can be modeled by a secondary stability theory (which studies the stability of a spatially periodic base flow); the K, H, and detuned types are initiated respectively from the 3-d fundamental modes, the 3-d subharmonic modes, and the combination modes.

The question we address is whether the path to transition via the sequence (i) primary and (ii) secondary instability mechanisms for compressible flows is viable. We attempt to answer this question, at least partially, by a parametric study of compressible secondary instability mechanisms.

Recently, El-hady (1989) [6] and Nayfeh (1989) [11] investigated the subharmonic secondary instability of compressible boundary layers for spatially developing disturbances. While El-hady studied the effect of compressibility from $M_\infty = 0$ to $M_\infty = 2.2$, Nayfeh extended the Mach number range to 4.5. El-hady found that the local effect of compressibility at a fixed Reynolds number and frequency is either stabilizing or destabilizing, depending on the amplitude of the primary wave and on the spanwise wavenumber of the secondary disturbance. However, when the primary growth and the diffusive growth of the mean flow are taken into account, he found that compressibility has an overall stabilizing influence on the subharmonic instability modes. Nayfeh found that increasing Mach number stabilizes the most unstable subharmonic wave. It should be pointed out that their analysis is based on a 2-d primary wave, although for compressible flows, the most unstable primary wave can be 2-d or oblique (i.e., the propagation direction of the primary wave phase fronts is inclined to the mean flow direction). In fact, for supersonic Mach numbers less than 3.0, the most unstable mode is always oblique. Clearly, for these Mach numbers, the effect of the primary wavevector angle on secondary instability mechanisms requires further study. In this paper, results are presented for both 2-d and oblique primary waves.

In addition to providing physical insight into the physics of the transition process, secondary instability theory has several potential practical objectives. The first is to refine the so-called e^N method, which is the most common and useful engineering tool used for transition prediction. The current e^N method is based on the primary disturbance which has the largest total streamwise growth from the lower branch neutral point to the location for the onset of transition. Bushnell [1] pointed out that a more refined e^N method should incorporate disturbances from primary, secondary and possibly other higher instability theories.

The e^N method has been quite successful for transition prediction in incompressible flows because of the following two reasons. First, the region from the incipient growth of TS disturbance to the onset of transition is dominated by the TS disturbance. Secondly, the primary disturbance which has the largest integrated growth leads to an explosive growth of 3-d disturbances which very rapidly yields to transition. However, whether the current e^N method will work in compressible flows remain uncertain. Secondary instability theory can shed light on this uncertainty.

Secondary instability theory also provides a much cheaper avenue for exploratory studies than do experiments or direct numerical simulations (DNS). Further, it provides a means to validate DNS (and vice versa). Relevant parameters (e.g. wavenumbers, frequencies, Re, etc) and the disturbance structure obtained from the theory can be used as the initial conditions for DNS, which can substantially reduce the computer time required to simulate strongly nonlinear phenomena.

Finally, if compressible secondary instability can indeed predict the correct space and time scales and the structures of the flow in the early stages of transition, then it can shed some light on the modeling of compressible transition. Since no compressible data (from experiments or DNS) for transitional Reynolds stresses is available, this work may provide a blueprint for future studies and experiments.

The paper is organized as follows. Section 2 contains the governing equations. The primary instability for compressible boundary layers is briefly reviewed in section 3. The secondary instability theory and its simplifying assumptions are formulated in section 4, and in section 5, the numerical methods are outlined. Section 6 contains the secondary instability results and the comparisons with direct numerical simulations. Finally, some conclusions are drawn in section 7.

II. Governing Equations

A schematic of the boundary layer flows is sketched in Fig. 1. In the chosen coordinate system, x, y and z denote the distance in the streamwise, spanwise and normal directions, respectively. We denote density, temperature and pressure respectively by ρ, T and p, and the velocity vector by $\mathbf{u}$. Lengths are non-dimensionalized with respect to the displacement thickness δ^*. The velocity, temperature, viscosity, and density are normalized with respect to their free-stream values (indicated by a subscript ∞). Pressure is normalized with respect to $\rho^*_\infty u^{*2}_\infty$. The equations governing the flow of a viscous compressible ideal gas are the compressible Navier-Stokes equations and the thermodynamic equation of state. With the aforementioned normalizations, these equations in dimensionless form are

$$\frac{\partial \rho}{\partial t} + \nabla\cdot(\rho\mathbf{u}) = 0 \tag{1}$$

$$\frac{\partial(\rho\mathbf{u})}{\partial t} + \nabla\cdot(\rho\mathbf{u}\mathbf{u}) = \frac{1}{Re}\nabla\cdot\sigma \tag{2}$$

$$\frac{\partial p}{\partial t} + \mathbf{u}\cdot\nabla p + \gamma p\nabla\cdot\mathbf{u} = \frac{1}{RePrM_\infty^2}\nabla\cdot(\mu\nabla T) + \frac{(\gamma-1)}{Re}\Phi \tag{3}$$

$$\gamma M_\infty^2 p = \rho T, \tag{4}$$

where

$$\sigma = 2\mu\left[\frac{1}{2}(\nabla\mathbf{u} + \nabla\mathbf{u}^T) - \frac{1}{3}(\nabla\cdot\mathbf{u})\mathbf{I}\right] \tag{5}$$

is the viscous stress and

$$\Phi = \frac{1}{2}(\nabla\mathbf{u} + \nabla\mathbf{u}^T) : \sigma \tag{6}$$

is the viscous dissipation function.

We assume a calorically perfect gas with the ratio of specific heats $\gamma(= C_p/C_v) = 1.4$. The Prandtl number $Pr = 0.70$, the Reynolds number Re is based on δ^*, and Sutherland's law is prescribed for the viscosity μ.

III. Primary Instability Theory

In this section, we consider the stability of an infinitesimally small primary disturbance superimposed on a steady, laminar mean flow. The mean profiles are the similarity solution of the 2-d compressible boundary layer equations applied to a semi-infinite, adiabatic flat plate. They are numerically computed using a spectral technique described in Streett, Zang and Hussaini [15]. The stability of high Mach number flows is found to be very sensitive to the mean flow. This implies that highly accurate mean flow profiles are required for meaningful stability calculations of high speed flows. Fig. 2a shows the mean velocity profiles versus y. Note that in terms of dimensionless y the boundary layer thickness mildly decreases with increasing M_∞, although, of course, the dimensional boundary layer thickness becomes significantly larger for higher free stream Mach numbers. Fig. 2b shows that for $M_\infty = 4.5$, there is a substantial variation of the mean temperature profile across the boundary layer, and that the maximum value of the temperature profile is about 4.5 times that of the mean velocity profile. The marked change in the temperature profiles can affect the stability behavior of boundary layers. The wall is adiabatic, as evidenced by the zero slope of the temperature profile.

Although the mean flow is in general a function of the x and y coordinates, we invoke, in the stability calculations, the classical parallel flow approximation where the streamwise variation of the mean flow is assumed negligible compared to its variation in the normal direction. Consequently the primary disturbance can be written in the modal form

$$\mathbf{q}_1 = \hat{\mathbf{q}}_1(y) \exp^{[i(\alpha x+\beta z-\omega t)]} + c.c. \tag{7}$$

where

$$\mathbf{q} = [u, v, w, T, \rho], \tag{8}$$

and the subscript 1 refers to the primary wave. α and β are respectively the wavenumbers in the streamwise and the spanwise directions, ω is the temporal frequency, $\hat{\mathbf{q}}_1(y)$ is the complex amplitude function which determines the transverse structure of the disturbance, and *c.c.* denotes the complex conjugate of the preceding term.

Two classess of theories are prevalent in the study of the stability characteristics of a small disturbance. In spatial theories, ω is real while α and β are complex. The real part of α is the streamwise wavenumber, while the imaginary part of α is the spatial growth rate. In temporal theories, α and β are real while ω is complex. The real and imaginary components of ω respectively determine the real frequency and the temporal growth rate of the wave. Eq. 7 then defines a wave with a real total wavenumber $\tilde{\alpha} = \sqrt{\alpha^2 + \beta^2}$ propagating with a complex phase velocity $\tilde{c} = \omega/\tilde{\alpha}$ in the direction $\theta = \tan^{-1}\beta/\alpha$. Temporal and spatial theories give identical results on the neutral curve only — where α, β and ω are all purely real and the growth rate is zero. When the growth rates are sufficiently small, an approximate relationship between the temporal and the spatial growth rate is given by the Gaster transformation [5]. In the present analysis, only temporally growing disturbances are considered.

Lees and Lins [8] pioneered the theoretical investigation of the linear stability of inviscid compressible flows. They found that a sufficient condition for the existence of a neutral subsonic disturbance (a neutral subsonic disturbance decays monotonically in the free-stream with increasing y) is the presence of an inflection point (which is the point where $\frac{d}{dy}(\rho_0 \frac{du_0}{dy}) = 0$; ρ_0 and u_0 are the mean density and the mean velocity). A comprehensive study of the linear stability of compressible flows is found in Mack [10]. More recent results on the stability of compressible boundary layers have been obtained by Malik [9]. For convenience, some of the relevant results are restated here. By solving the full disturbance equations (including the viscous and conductivity terms) numerically, Mack discovered that several unstable modes may coexist in a high Mach number compressible boundary layer.

The first mode is the compressible extension of the TS mode found in the incompressible boundary layer. At low Mach numbers, this mode is primarily viscous (the maximum amplification rate increases with decreasing Reynolds number). It is known that compressible boundary layers on insulated flat plates have a generalized inflection point. At higher Mach numbers, inflectional instabilities become important because the generalized inflection point is located farther away from the wall. Therefore, as the Mach number increases, the instability mechanism progressively switches from the viscous to the inviscid type (where amplification rate increases with increasing Re), although compressibility has in general a stabilizing influence. In fact, when M_∞ approaches about 2.2, the viscosity is stabilizing for all Reynolds numbers, and inviscid instability modes are the most unstable. In contrast to subsonic flows, the most unstable first mode is oblique for supersonic flows.

Higher instability modes exist when the free stream Mach number becomes larger than 2.2. These modes do not require a generalized inflection point, and they are characterized by phase velocities close to unity and high frequencies (or wavenumbers). The higher modes depend on the existence of a region where the local Mach number of the mean flow (relative to the phase velocity $\tilde{c}$) is supersonic. The first of the higher modes is called the second mode. It first appears when M_∞ is approximately 2.2, but is not dominant until M_∞ reaches about 3.7. The second mode reaches a peak amplification rate when $M_\infty \approx 4.5$. It is the most unstable of the higher modes, and is most unstable when it propagates in the mean flow direction.

The influence of M_∞ on the eigenfunctions of the first mode primary wave is illustrated in Fig. 3 which shows that at $M_\infty = 4.5$, the maximum value of the temperature perturbation is about 15 times larger than the corresponding velocity fluctuation. This is in contrast to subsonic flows where the streamwise velocity perturbation is the dominant one. A side by side comparison between typical eigenfunctions of the first and second modes at $M_\infty = 4.5$ is shown in Fig. 4. We note that although the vertical velocity perturbation for the first mode is negligible, it is not insignificant for the second mode. Another feature of note is that the second mode disturbance decays much faster in the freestream than does the first mode wave.

IV. Secondary Instability Theory

The instability of a base flow consisting of a small amplitude primary disturbance superimposed on a parallel mean flow is called secondary instability. We begin with a physical description of how a small monochromatic primary disturbance propagates downstream in a boundary layer. As the disturbance crosses the lower branch of the neutral stability curve, its amplitude begins to grow exponentially according to linear (primary) spatial instability theory. Assuming nonlinear effects remain negligible, the disturbance continues to amplify linearly until it reaches the upper branch (also known as branch two) where its local amplification rate is again zero and its amplitude reaches a maximum value. Farther downstream, the disturbance begins to decay. When nonlinear effects are negligible, it is physically realistic to use a primary disturbance which is located near branch two as input to a secondary instability theory (since the stability characteristics of a linear spatial instability wave, which achieves its maximum amplitude at branch two, can be accurately represented by a linear temporal wave in the neighborhood of the neutral point).

The flow in the presence of the primary disturbance is periodic in the streamwise direction, and hence its stability is governed by Floquet theory. For incompressible flows, it is known that the periodic base flow is very unstable to 3-d secondary disturbances [7].

We now apply Herbert's approach to compressible flows with an oblique primary wave. When the primary wave is oblique, it is appropriate to use a new-axis, $\tilde{x}_1$, which is aligned in the propagation direction of the primary wave. The $\tilde{z}_1$ axis is perpendicular to the wavevector of the primary wave and is in the plane of the plate. Only when the primary wave is two dimensional is the $\tilde{z}_1$ axis oriented in the spanwise direction

Specifically, in the $(\tilde{x}_1, \tilde{y}_1 = y, \tilde{z}_1)$ coordinate system (Fig. 1), the mean velocity profile becomes

$$\mathbf{u}_0 = (u_0 \cos\theta, 0, -u_0 \sin\theta) \tag{9}$$

and the primary velocity disturbance takes the form

$$\mathbf{u}_1 = (\tilde{u}_1, \tilde{v}_1, \tilde{w}_1) e^{i\tilde{\alpha}(\tilde{x}_1 - \tilde{c}t)} + c.c. \tag{10}$$

where

$$\tilde{u}_1 = \hat{u}_1 \cos\theta + \hat{w}_1 \sin\theta \tag{11}$$

$$\tilde{v}_1 = \hat{v}_1 \tag{12}$$

$$\tilde{w}_1 = \hat{w}_1 \cos\theta - \hat{u}_1 \sin\theta. \tag{13}$$

The tilde refers to a quantity in the new coordinate system, the hat corresponds to a quantity in the old system, and *c.c.* denotes the complex conjugate of the preceding term. Note that there are two effects associated with an oblique primary wave. First, there is a mean velocity component in the $\tilde{z}_1$ direction. Second, the effective free stream Mach number in the propagation direction of the primary wave is reduced to $M_\infty \cos\theta$ from M_∞.

For a small primary amplitude, A, the base flow, say, for instance, the base temperature $\tilde{T}_b$, can formally be expanded as

$$\tilde{T}_b(\tilde{x}_1, y, t) = \left\{\tilde{T}_0(y) + A^2 \tilde{T}_0^1(y)\right\} + A\left\{\tilde{T}_1(y) + A^2 \tilde{T}_1^1(y)\right\} e^{i\tilde{\alpha}\tilde{x}_1} + \left\{A^2 \tilde{T}_2^1\right\} e^{2i\tilde{\alpha}\tilde{x}_1} + O(A^4) \tag{14}$$

where $\tilde{T}_0^1, \tilde{T}_1^1, \tilde{T}_2^1$ are the corrections due to the nonlinear self-interaction of the primary wave. Similar expansions apply for other variables. When the primary wave saturates, its amplitude can in principle be obtained from a nonlinear analysis or from direct numerical simulations [12]. Following Herbert's analysis of incompressible wall boundary layers, we assume that:

1. The nonlinear self-interaction of the primary wave does not significantly distort the shape of the mean flow and of the primary wave. For incompressible flows, it is found that this distortion is minimal even for streamwise velocity disturbances of up to 10% (see Santos [14], page 11).

2. The amplitude of the primary wave remains constant during the evolution of the secondary disturbance. In other words, the growth of the primary wave is frozen by setting the imaginary part of $\tilde{c}$, $\tilde{c}_i$, to zero. The primary merely acts as a catalyst which feeds energy from the mean flow to the (secondary) disturbance. This assumption can be justified a posteriori by accepting only those secondary disturbances which have growth rates much larger than that of the primary wave. Consequently, this assumption also forbids the construction of neutral curves for the secondary disturbance.

3. The amplitude, ε, of the secondary disturbance is assumed sufficiently small to ensure that linearization of the governing equations with respect to ε is permissible. A consequence of this assumption is that the feedback from the secondary disturbance to the primary wave is neglected. A complete analysis of this feedback mechanism for incompressible flows is detailed in Crouch [2].

With these assumptions, the dependent variable, $\mathbf{q}$, is decomposed according to

$$\mathbf{q} = \tilde{\mathbf{q}}_b + \epsilon \mathbf{q}_2 \tag{15}$$

where

$$\mathbf{q}_b = \tilde{\mathbf{q}}_0(y) + A\{\tilde{\mathbf{q}}_1(y) e^{i\tilde{\alpha}(\tilde{x}_1 - \tilde{c}_r t)} + c.c\} + O(A^2), \tag{16}$$

$$\tilde{\mathbf{q}}_0 = [u_0 \cos\theta, 0, -u_0 \sin\theta, T_0, \rho_0]^T, \tag{17}$$

$$\tilde{\mathbf{q}}_1 = [\tilde{u}_1, \tilde{v}_1, \tilde{w}_1, \tilde{T}_1, \tilde{\rho}_1]^T, \tag{18}$$

$\tilde{c}_r$ is the real part of $\tilde{c}$, and the subscript b indicates a base flow quantity. The viscosity, assumed a function of the temperature alone, is Taylor expanded according to

$$\mu(T) = \mu_0 + \mu_0'(AT_1 + \epsilon T_2) + \mu_0''(T_1 T_2 A\epsilon) + O(A^2, \epsilon^2), \tag{19}$$

where the primes denote differentiation with respect to the mean temperature.

Since $\tilde{\mathbf{q}}_1$ is an eigenfunction, the amplitude of the primary disturbance is not uniquely defined from a linear stability analysis. In the (linear) secondary instability analysis of El-Hady [6] and Nayfeh [11], the eigenfunction is normalized so that A corresponds directly to the maximum r.m.s. value of the streamwise velocity perturbation, which is the dominant perturbation in subsonic flows. For Mach numbers that are less than 2.0, the same normalization is used here, i.e.,

$$\max_{0 \le y < \infty} |\hat{u}_1(y)|^2 = 1/2 \tag{20}$$

We caution the reader that the above normalization may invalidate the use of the shape assumption in the supersonic and hypersonic regimes. For example, at $M_\infty = 4.5$, the maximum temperature perturbation is an order of magnitude larger than the corresponding maximum velocity fluctuation. This means that if A is defined in terms of the velocity perturbation, the total magnitude of the temperature perturbation AT_1 may no longer be smaller than that of the mean temperature T_0, and consequently the neglect of terms of $O(A^2)$ and higher in the construction of the base flow (16) would not be justified. In order to avoid this possible inconsistency, we define A, for Mach numbers ≥ 2, so that it is the maximum r.m.s. value of the largest perturbation (which happens to be the temperature perturbation in all cases described here) i.e.,

$$\max_{0\leq y<\infty} |\hat{\mathbf{q}}_1(y)|^2 = 1/2 \tag{21}$$

The above normalization ensures that when A is small, the rms of all primary variables are also small. We note in passing that a normalization which is less sensitive to the location of the grid points is by normalizing the primary eigenfunction so that its magnitudes have a specific area, for example,

$$\int_0^\infty |\hat{T}_1(y)|^2 = 1/2\, dy.$$

We introduce a new coordinate system $\tilde{x} = \tilde{x}_1 - \tilde{c}_r t, \tilde{y} = y, \tilde{z} = \tilde{z}_1$ which moves with the phase velocity, $\tilde{c}_r$, of the primary wave. In this moving frame of reference, the coefficients of the secondary disturbance equations, which depend only on the periodic base flow, are independent of both $\tilde{z}$ and t. Thus, we can assume a normal mode representation in $\tilde{z}$ and t for the secondary disturbance and write

$$\mathbf{q}_2 = \tilde{\mathbf{q}}_2(\tilde{x}, \tilde{y}) e^{\sigma t} e^{i\beta_2 \tilde{z}} \tag{22}$$

where β_2 is the wavenumber in the $\tilde{z}$ direction. When ε is sufficiently small, the stability of the secondary disturbance is governed by a system of linear partial differential equations. These equations are obtained by substituting Eqs. 15-19 into Eqs. 1-3, and keeping only terms linear in ε. Apart from a complicated $\tilde{y}$ dependence, these equations are of the classical Floquet type because the coefficients are periodic in $\tilde{x}$. Accordingly, the structure of the secondary disturbance in the $\tilde{x}$ direction has the following general Floquet form (in terms of a Fourier series):

$$\tilde{\mathbf{q}}_2 = e^{\gamma\tilde{x}} e^{ie_h \frac{\tilde{\alpha}}{2}\tilde{x}} \sum_{j=-\infty}^{\infty} \mathbf{q}_{2,j}(\tilde{y}) e^{ij\tilde{\alpha}\tilde{x}}, \tag{23}$$

where γ is the characteristic exponent, e_h is a parameter whose value distinguishes the various types of secondary instabilities, $\mathbf{q}_{2,j}$ is the shape function of a mode whose wavenumber in the $\tilde{x}$ direction is given by $\alpha_2 = e_h\tilde{\alpha}/2 + \gamma + j\tilde{\alpha}$. The fundamental resonance is associated with the harmonic series ($e_h = 0$) whose period equals the primary wavelength (i.e., $2\pi/\tilde{\alpha}$), while the subharmonic resonance is determined by the subharmonic series ($e_h = 1$) whose period is twice the primary wavelength. When $0 < |e_h| < 1$, the secondary waves are called combination resonance modes (or detuned modes). They can have an arbitrary wavenumber in the $\tilde{x}$ direction, depending on the value of e_h.

We consider only temporal theory, which implies that $\gamma = 0$ and that $\sigma \neq 0$ is the complex eigenvalue to be found. The real part of σ, σ_r, is the growth rate, and the imaginary part of σ, σ_i, defines the frequency of the secondary disturbance in the moving coordinate frame. Note that, for a given class of secondary waves, all the modes $\mathbf{q}_{2,j}$ grow or decay at the same rate and travel with the same frequency according to Eqs. 22-23. The growth rates are the same both in the moving frame and in the laboratory frame. When σ is real, the secondary and the primary disturbances travel with the same phase velocity in the $\tilde{x}$ direction. They are phase locked. For complex σ, the phase velocities of the two disturbances are different.

Substitution of Eqs. 15, 22 and 23 into the linearized disturbance equations yields an infinite set of ODE's governing the stability of the secondary disturbance. Because the governing equations for compressible flows have cubic convective nonlinearities and because the viscosity is a nonlinear function of the temperature, terms of $O(A^2\varepsilon)$ and higher are present. These higher order terms are neglected in the analysis because the base flow is only approximated to $O(A)$, as are the base flows of Herbert [7], El hady [6], and Nayfeh [11]. These secondary disturbance equations form a generalized complex eigenvalue problem

$$\left(\mathbf{A}_1 D^2 + \mathbf{A}_2 D^1 + \mathbf{A}_3\right)\phi = \sigma \mathbf{A}_4 \phi, \tag{24}$$

where D^p indicates a p-fold differentiation with respect to $\tilde{y}$. The **A**'s, which are function of the base flow alone, are complex, and ϕ is the vector of the unknown $\mathbf{q}_{2,j}$. Since ϕ is an eigenfunction, its amplitude is determined only up to an arbitrary complex constant.

A numerical solution to Eq. 24 requires the truncation of the Fourier series (Eq. 23). For an N mode truncation, the size of the **A**'s is $5N \times 5N$. When N is an odd integer, the secondary disturbance takes the form

$$\mathbf{q}_2 = e^{\sigma t} e^{i\beta_2 \tilde{z}} \mathrm{e}^{\gamma \tilde{x}} \mathrm{e}^{i e_h \frac{\tilde{\alpha}}{2} \tilde{x}} \sum_{j=-\frac{N-1}{2}}^{\frac{N-1}{2}} \mathbf{q}_{2,j}(\tilde{y}) \mathrm{e}^{ij\tilde{\alpha}\tilde{x}} . \tag{25}$$

For an even N, the secondary disturbance is represented by

$$\mathbf{q}_2 = e^{\sigma t} e^{i\beta_2 \tilde{z}} \mathrm{e}^{\gamma \tilde{x}} \mathrm{e}^{i e_h \frac{\tilde{\alpha}}{2} \tilde{x}} \sum_{j=-\frac{N}{2}}^{\frac{N-2}{2}} \mathbf{q}_{2,j}(\tilde{y}) \mathrm{e}^{ij\tilde{\alpha}\tilde{x}} . \tag{26}$$

Accordingly, to lowest order, the fundamental and the detuned disturbances can be represented by 3 Fourier modes ($N = 3$) according to

$$\mathbf{q}_2 = e^{\sigma t} e^{i\beta_2 \tilde{z}} e^{(i e_h \tilde{\alpha}/2)\tilde{x}} (\mathbf{q}_{2,-1} \mathrm{e}^{-i\tilde{\alpha}\tilde{x}} + \mathbf{q}_{2,0} + \mathbf{q}_{2,1} \mathrm{e}^{i\tilde{\alpha}\tilde{x}}) \tag{27}$$

and the subharmonic disturbance by 2 Fourier modes ($N = 2$) according to

$$\mathbf{q}_2 = e^{\sigma t} e^{i\beta_2 \tilde{z}} (\mathbf{q}_{2,-1} \mathrm{e}^{-i(\tilde{\alpha}/2)\tilde{x}} + \mathbf{q}_{2,0} \mathrm{e}^{i(\tilde{\alpha}/2)\tilde{x}}) \tag{28}$$

For incompressible flows, the aperiodic $q_{2,0}$ term in Eq. 27 is known to give rise to both a mean flow distortion and a spanwise periodic longitudinal vortex structure associated with the peak-valley splitting in a K type breakdown process. It turns out (see section 6) that when the primary wave is 2-d, the truncation levels defined by Eqs. 27-28 are usually sufficient to resolve the streamwise structure of the secondary disturbance, whether the flow is compressible or not. However, when the primary wavevector is inclined at a significant angle to the mean flow direction, higher Fourier modes are required.

The stability calculations for compressible flows are substantially more computer intensive those of incompressible flows because all the dependent variables are now coupled and the number of grid points required generally increases with increasing M_∞. A spectral representation (see next section) of Eq. 24 leads to a generalized matrix eigenvalue problem whose eigenvalues require $O(5 \times N \times N_c)^2$ storage and $O(5 \times N \times N_c)^2$ operations — where N_c is the number of grid points. When the structure of the compressible secondary disturbance in the $\tilde{x}$ direction is represented by more than three Fourier modes, it becomes impractical to compute these eigenvalues (using a global method) in a parametric study, especially for the higher Mach number flows. Therefore, our computations are done using Eqs. 27-28, unless otherwise indicated. The effect of the neglected higher Fourier modes on σ is only examined in some selected cases, although some insight into the convergence of the Fourier series can also be obtained from DNS.

The appropriate boundary conditions for the secondary disturbances are

$$(u_2, v_2, w_2, T_2) = 0 \quad at \quad \tilde{y} = 0 \tag{29}$$

$$(u_2, v_2, w_2, T_2) \rightarrow 0 \quad as \quad \tilde{y} \rightarrow \infty \tag{30}$$

The boundary conditions on the density disturbances are not explicitly imposed since they satisfy the continuity equation. We next outline the numerical algorithm.

V. Numerical Method

The system of homogeneous equations Eq. 24 plus the homogeneous boundary conditions, Eqs. 29-30, lead to a dispersion relation of the form

$$\sigma = \sigma(\alpha_2, \beta_2). \tag{31}$$

The eigenvalue, σ, is obtained numerically using a spectral collocation technique based on Chebyshev polynomials. The collocation points for all the dependent variables are the Gauss-Lobatto points. These points, which are the extrema of the highest Chebyshev polynomial retained, are defined by

$$\eta_j = \cos\frac{j\pi}{\mathcal{N}} \quad j = 0, 1, ..., \mathcal{N} \tag{32}$$

where $\mathcal{N}$ is highest order Chebyshev polynomial. In order to provide an adequate resolution near the wall and the critical layer, the physical domain y is mapped onto the Chebyshev domain η through two different transformations.

The first transformation, upon which most of the results reported in this paper are based, maps the finite physical domain $y \in [0, y_{max}]$ onto $\eta \in [-1, 1]$ through a combination of hyperbolic tangent and algebraic stretchings according to

$$\psi + t_\epsilon \tanh\left(\frac{\psi - \psi_0}{\Delta\psi}\right) = \frac{\eta - \eta_0}{\Delta\eta} \tag{33}$$

$$y = \frac{y_{1/2} y_{max}(1 + \psi)}{y_{max} - \psi(y_{max} - 2y_{1/2})} \tag{34}$$

where

$$\Delta\psi = \frac{d\psi}{dy}|_{y=y_0} \Delta y_0 \,. \tag{35}$$

Here t_ϵ is a concentration parameter which clusters nodes about ψ_0. If $t_\epsilon = 0$, there is no stretching due to the influence of the hyperbolic tangent term. Δy_0 is the width of the concentration region in the physical domain. The far field boundary of the discretized physical domain is located at y_{max}, and half of the nodes are distributed between $y = 0$ and $y = y_{1/2}$. Dirichlet conditions are imposed on both the primary and the secondary disturbances at $y = y_{max}$ where all variables, except the density, are set to zero. The determination of the adjustable constants y_{max}, $y_{1/2}$, t_ϵ and Δy_0 is empirical; more details are given in [4]. For $M_\infty \leq 1.6$, $y_{max} = 100$, $y_{1/2} = 2$, and $t_\epsilon = 0$. When $M_\infty = 4.5$, two sets of parameters are used; for first mode calculations, runs are performed with $y_{max} = 30$, $y_{1/2} = 1$, $t_\epsilon = 0.8$, $y_0 = 1.2$ and $\Delta y_0 = 0.4$, while $y_{max} = 15$, $y_{1/2} = 1$, $t_\epsilon = 0.8$, $y_0 = 1.2$ and $\Delta y_0 = 0.4$ are for second mode calculations. A lower value of y_{max} for second mode calculations reflects the faster decay of the second mode eigenfunctions in the free stream compared to that of the first mode waves.

The second mapping transforms $y \in [0, \infty]$ onto $\eta \in [1, 0]$ via

$$\eta = \frac{l_1}{2(y + l_1)} + \frac{1}{2}\exp[-\frac{y^n}{l_2}]. \tag{36}$$

When $n = 1$ and $l_1 = 0$, the mapping reduces to the classical exponential mapping. For given l_1 and l_2, n controls the number of grid points in the neighborhood of the critical point (near $y = 1$). Increasing n adds more nodal points around the critical layer region. The parameters l_2 and n redistribute some of the nodal points near $y = 0$ to the critical layer. The point $y = 0$ is mapped onto $\eta = 1$, while the point $y = \infty$ is mapped onto $\eta = 0$ (not a collocation point). All variables are expanded in odd polynomials to implicitly satisfy the boundary conditions at $y = \infty$. Calculations are performed with $l_1 = 7$, $l_2 = 7$, and $n = 3$.

A global method, based on a modified QZ algorithm [16], is used to obtain all the eigenvalues of the discrete system of linear equations. We then select the most unstable eigenvalue and use it as input to a local procedure, which is based on an inverse Rayleigh solver. The local method generates a more accurate eigenvalue and its corresponding eigenfunction. The eigenvalues are at least accurate to 5 decimal places for primary eigenfunctions and to 4 decimal places for a secondary eigenfunctions. Since the accuracy of the secondary disturbance depends on the accuracy of the primary wave but not conversely, a more stringent convergence criterion is imposed on the primary wave to ensure that its derivatives are determined with sufficient accuracy. In all cases, the ratio of the maximum of the absolute value of the last three Chebyshev coefficients over the maximum of the absolute value of the first half Chebyshev coefficients is always less than 10^{-4}; this procedure should exclude any spurious modes, unless they happen (very unlikely) to be well resolved.

VI. Results and Comparison with Direct Numerical Simulations

A. Code validation

In the absence of experimental data for compressible flows, the secondary instability code is validated against the established incompressible results of Herbert et al [7] and against results from direct numerical simulations of the full compressible Navier-Stokes equations. For convenience, the verification for incompressible flow is reported using the reference length $L = (\nu^*_\infty x^*/u^*_\infty)^{1/2}$ instead of δ^*. The parameters used (in Herbert's units) are $\alpha = 0.20335, \beta = 0, A = 1\%, \beta_2 = 0.2, M_\infty = 10^{-6}, Re = 606$ and $T_\infty = 520^0 R$. The results are tabulated below:

Detuning	Number of Fourier Modes	45 points		55 points	
		$10^3\ \sigma_r$	$10^3\ \sigma_i$	$10^3\ \sigma_r$	$10^3\ \sigma_i$
$e_h = 1$	2	8.1177	0	8.1177	0
subharmonic	3	8.1568	0.0145	8.1568	0.0144
mode	4	8.1958	0	8.1958	0
$e_h = 0.5$	2	6.1811	1.6457	6.1811	1.6456
detuned	3	6.4067	1.4818	6.4067	1.4816
mode	4	6.4185	1.4711	6.4183	1.4710
$e_h = 0$	2			-1.7356	2.0434
fundamental	3	3.6388	0	3.6387	0
mode	4	3.6498	-0.0102	3.6495	-0.0103

Table 1

A side by side comparison between the above table and Table 1 of Herbert et. al. [7] shows that the eigenvalues are in agreement to at least 5 decimal places. Except for Table 1, all computations are based on δ^*.

The verification for compressible flows is performed using a code described in detail in Erlebacher and Hussaini [4]. For completeness, a brief description of the method is outlined here. Periodic boundary conditions in $\tilde{x}$ and $\tilde{z}$ are imposed where $\tilde{x}$ is in the propagation direction of the 2-d or 3-d primary wave. The computation domain has dimensions $L_{\tilde{x}} = 2\pi/\alpha^*$ and $L_{\tilde{z}} = 2\pi/\tilde{\beta}$ in the $\tilde{x}$ and $\tilde{z}$ directions respectively, where $\alpha^* = \tilde{\alpha}$ for the fundamental instability and $\alpha^* = \tilde{\alpha}/2$ for the subharmonic instability. In the normal direction, the finite physical domain $y \in [0, y_{max}]$ is mapped onto $\eta \in [-1, 1]$ according to Eqs. 33-35. The spatial discretization is based on a spectral collocation method with Fourier expansions in the $\tilde{x}$ and $\tilde{z}$ directions, and Chebyshev expansions in the normal direction, $\tilde{y} = y$. Velocities satisfy no-slip boundary conditions and the wall is adiabatic. Dirichlet boundary conditions are imposed at $y = y_{max}$. Initially, the flow consists of a parallel mean flow plus the primary and the secondary disturbances. Time marching is achieved with a third order Runge Kutta method. The growth rate g_{jl} of the disturbances is monitored through

$$g_{jl} = \frac{1}{2E_{jl}} \frac{dE_{jl}}{dt} \tag{37}$$

where

$$E_{jl}(t) = \int_0^\infty (|u_{jl}|^2 + |v_{j,l}|^2 + |w_{j,l}|^2) dy, \tag{38}$$

u_{jl}, v_{jl} and w_{jl} are the Fourier coefficients of the u, v and w velocity components, respectively. The subscripts j and l denote the Fourier components in the $\tilde{x}$ and $\tilde{z}$ direction, respectively.

Comparisons between theory and DNS are performed at Mach 1.6 (Fig. 5a) and Mach 4.5 (Fig. 5b). At $M_\infty = 1.6$, the parameters are $Re = 1675$, $T_\infty = 520^0R$, $(\alpha, \theta) = (0.24, 10^0)$, $\beta_2 = 0.4$, $e_h = 0$, $N = 3$, $A = 0.015$, and $\varepsilon = 0.0015$. The calculations at $M_\infty = 4.5$ are for $Re = 10000$, and $T_\infty = 110^0R$, $(\alpha, \theta) = (2.52, 0^0)$, $\beta_2 = 2.1$, $e_h = 1$, $N = 2$, $A = 0.06$, and $\varepsilon = 0.006$. Here ε is the initial amplitude of the secondary disturbance used in the DNS, and time is normalized with respect to the period of the primary wave. The following two tables represent respectively samples of each comparison at $M_\infty = 1.6$ (Table 2) and $M_\infty = 4.5$ (Table 3):

time	primary growth rate $\times 10^4$		secondary growth rate $\times 10^2$	
	theory	DNS	theory	DNS
0.000	1.919	1.911	1.127	1.112
0.010	1.919	1.799	1.127	1.111
0.023	1.919	1.947	1.127	1.112

Table 2

time	primary growth rate $\times 10^3$		secondary growth rate $\times 10^2$	
	theory	DNS	theory	DNS
0.000	2.867	3.023	2.506	2.500
0.640	2.867	3.014	2.506	2.504
1.022	2.867	2.873	2.506	2.492

Table 3

Fig. 5a represents the dominant fundamental mode at $M_\infty = 1.6$ and $A = 1.5\%$, which arises from a primary disturbance propagates at 10^0 to the mean flow direction, while Fig. 5b represents the most amplified subharmonic based on a 2-d, second mode primary disturbance with $A = 6\%$. The figures show that the theoretical growth rates of primary and secondary disturbances compare well with the growth rates obtained by DNS. There is a small difference between the Prandtl number used in theory (0.70) and in DNS (0.72). This difference, although small and unintentional, may partly account for the small discrepancies between theoretical and numerical results. For both the Mach 1.6 and Mach 4.5 cases, the secondary disturbances are stable in the absence of the primary disturbance. However, the presence of the finite amplitude primary disturbance triggers a strong secondary instability with the growth rate of the secondary disturbance far exceeding that of the primary.

B. *Parametric studies*

The free stream Mach number M_∞ affects secondary instability directly through the (secondary) disturbance equations and indirectly through modification of the mean flow and primary wave. The influence of M_∞ on secondary instability is studied in this section.

VI.2.1. Subsonic flows

We begin with a study of the secondary instability at $M_\infty = 0.8$. Fig. 6 depicts the growth rate versus the spanwise wavenumber for the three types of secondary instability waves at $Re = 1675$, $T_\infty = 520^0 R$, $\alpha = 0.29$, $\beta = 0$, and two primary wave amplitudes: $A = 1.5\%$ and $A = 0.5\%$. The parameters, Re and T_∞, are approximately the same as those given in [6]. The primary wave is 2-d, slightly unstable, and is located near branch two of a neutral curve with a growth rate of 0.0006. Although the subharmonic and the fundamental disturbances travel with the phase velocity of the primary, the detuned disturbance does not. Additionally, the following salient features may be extracted from this figure: (1) There is a wide band of highly unstable 3-d secondary disturbances whose growth rates increase with increasing primary wave amplitude. As $\beta_2 \to 0$, the secondary disturbances rapidly become stable. Since 2-d (i.e., $\beta_2 = 0$) secondary disturbances are unstable in free shear layers [13], we conclude that the presence of the wall at $y = 0$ can damp the secondary disturbances with long spanwise wavelengths. (2) There is a preferred band of spanwise wavenumbers within which the secondary growth rate has a local maximum. Increasing the primary wave amplitude mildly increases the preferred spanwise wavenumber and significantly widens the range of β_2 over which a secondary disturbance is unstable. At $A = 1.5\%$, the spanwise wavenumber of the most amplified subharmonic approximately equals the streamwise wavelength of the primary wave. As the type of instability changes from subharmonic to fundamental, (i.e., as e_h decreases from 1 to 0), the preferred spanwise wavenumber increases slightly. (3) The subharmonic modes are the most unstable, followed by the detuned modes and then the fundamental modes. The preceding result is consistent with the classical scenario of the

H-type breakdown in which the subharmonic modes dominate when the primary amplitude is low.

The subharmonic growth rates from Fig. 6 are then compared to two sets of incompressible results. Fig. 7a illustrates the first comparison using Re $= 1675$, $T_\infty = 520^0 R$, $\alpha = 0.29$, and $\beta = 0$. The primary growth rates at $M_\infty = 0.0$ and $M_\infty = 0.8$ are 0.0028 and 0.0006 respectively. For clarity, let β_{max} be the spanwise wavenumber of the most amplified subharmonic. An interesting feature is that subsonic compressibility destabilizes the subharmonic waves with $\beta_2 \geq \beta_{max}$. At $A = 0.5\%$, compressibility appears to have a stabilizing influence for the disturbances with $\beta_2 < \beta_{max}$.

The second set of calculations is performed using $\alpha = 0.29$ and two different Reynolds numbers: $Re = 2700$ for $M_\infty = 0.0$ and $Re = 1675$ for $M_\infty = 0.8$. These Reynolds numbers are chosen to ensure that the primary growth rates at both Mach numbers are approximately the same ($\omega_i = 0.0006$). The results for the subharmonic growth rate versus the spanwise wavenumber are plotted in Fig. 7b. In contrast to the results in Fig. 7a, compressibility now has a stabilizing influence. Therefore, although there is a strong growth of 3-d secondary disturbances at subsonic Mach numbers, the particular effect of compressibility on *local* subharmonic growth rates is unclear (we remark that the growth rates have been scaled with u^*_∞/δ^* which changes with M_∞). It can either have a stabilizing or a destabilizing influence, depending on how the comparison with incompressible flow is made. Such a comparison is only meaningful when the following conditions are met (i) when all quantities are expressed in dimensional form, (ii) when the free stream disturbances are coupled with the primary disturbances (i.e a receptivity problem), and (iii) when the *total* growth of the mean flow and the primary disturbance is incorporated into the calculations. The point is that since the primary wave amplitude (which is responsible for the onset and growth of the secondary disturbance and which is in itself sensitive to the free-stream enviroment) cannot be uniquely determined from stability analysis, it is meaningless to make any general conclusions on the overall influence of compressibility on secondary instabilities. Henceforth conclusions about the secondary instabilities in this paper are local in nature and are based on the primary wave amplitudes (and other flow parameters) which are assumed known.

VI.2.2. Supersonic flows

The subharmonic and the fundamental growth rates at $M_\infty = 1.6$, $Re = 1675$, $T_\infty = 520^0$ R, $\alpha = 0.24$, and $\beta = 0$ are plotted against β_2 in Fig. 8 and Fig. 9 respectively. The primary mode is slightly unstable, located near branch two of the neutral curve. There is a broadband of 3-d secondary disturbances whose growth rates are large (compared to the maximum primary growth rate which approximately equals 0.003) and increase with increasing A. The results lead us to believe that secondary instability mechanisms at $M_\infty = 1.6$ play a significant role in the boundary-layer transition and that the process of laminar breakdown is similar to the mechanisms found in incompressible flows. The spanwise wavelength of the most unstable secondary disturbance is about 60% of the streamwise wavelength of the primary disturbance, and this wavelength is almost insensitive to the primary amplitude.

Fig. 10 shows the influence of the primary amplitude A on σ_r. The parameters used are identical to those of Figs. 8 and 9 when $\beta_2 = 0.4$ (i.e., the spanwise wavenumber of the most dangerous secondary disturbance). Here the fundamental instability is stronger than the subharmonic instability when A is larger than 2.5%, while the converse is true for smaller values of A.

Next the secondary instability is studied $M_\infty = 4.5, T_\infty = 110^0 R, Re = 10000$, and two values of α : 0.6 for a first mode calculation and 2.52 for a second mode calculation for four primary amplitudes ($A = 0\%, 2\%, 3\%, 6\%$). The growth rates of the 2-d primary waves for the first mode and the second mode calculations are 0.002087 and 0.003185, respectively. The first mode primary wave, which is the same as that reported in [3], is the most amplified 2-d mode. The second mode primary wave is chosen so that it is located near branch two. For these parameters, no evidence of the fundamental secondary instability can be found. The subharmonic instability results are shown in fig. 11a (first mode) and fig. 11b (second mode).

In Fig. 11a, it is interesting to note that when the primary amplitude is non-zero, there are two humps in the curve of σ_r versus β_2. Hump one has a complex σ whereas hump two has a real σ. The growth rates of the unstable modes whose spanwise wavelengths are longer than the streamwise wavelength of the primary mode are marginally affected by the primary amplitude; in other words, these waves are essentially the 3-d primary (subharmonic) instability modes. The unstable waves on hump two are secondary instability waves. While increasing the primary amplitude marginally stabilizes hump one, it significantly destabilizes hump two. At $A = 6\%$, the growth rates of the most amplified primary (subharmonic) and secondary (subharmonic) modes are comparable.

Fig. 11b demonstrates that the subharmonic instabilities which originate from the second mode primary wave differ substantially from the corresponding first mode case. Here σ_r versus β_2 curve has only one maximum. The eigenvalue σ is real for all values of β_2, and the subharmonic in the absence of the primary disturbance is stable. Increasing the primary wave amplitude destabilizes the subharmonic and dramatically widens the range of spanwise wavenumber over which a subharmonic is unstable. The most amplified subharmonic, whose spanwise wavenumber $\beta_2 \approx 2.1$ is rather insensitive to A, has a spanwise wavelength approximately equal to 80% of the streamwise wavelength of the primary. As A changes from 2% to 6%, the growth rate of the most amplified subharmonic is increased by 135% (from 0.0075 to 0.0251). Since the maximum growth rates of both the primary and the secondary disturbances for the second mode calculations are considerably higher than the corresponding first mode calculations, we conjecture that boundary-layer transition at $M_\infty = 4.5$ will occur (in all likelihood) via second mode disturbances.

The convergence of the Fourier modes for the most unstable subharmonic mode from Fig. 11b, together with the fundamental and the detuned modes, is performed. (To the authors best knowledge, such a convergence study has never been done for compressible secondary instability theory). As evidenced from Table 4, the streamwise structure of the subharmonic disturbance can be accurately captured by using only two Fourier modes, just as in incompressible flows.

Detuning	Number of Fourier Modes	65 points	
		$10^2\ \sigma_r$	$10^2\ \sigma_i$
$e_h = 1$	2	2.506	0
subharmonic	3	2.502	0.002
mode	4	2.500	0
$e_h = 0.5$	2	1.929	0.618
detuned	3	1.918	0.618
mode	4	1.918	0.617
$e_h = 0$	2		
fundamental	3	stable	
mode	4		

Table 4

Fig. 12 shows σ_r as a function of the detuning parameter at $M_\infty = 4.5$ using 3 Fourier modes (i.e., $N = 3$), $\alpha = 2.52$, $\beta = 0$, $A = 0.06$, $T_\infty = 110^0R$, $Re = 10000$, and $\beta_2 = 2.1$. It reveals that σ_r is a continuous function of e_h and that there is a broad band of highly unstable modes. The subharmonic mode has the largest growth rate, while the fundamental mode is stable.

The corresponding influence of the detuning parameter on the frequency shift σ_i is illustrated in Fig. 13. While the subharmonic mode has real σ (which implies that it travels synchronously with the primary mode), the detuned and fundamental modes have complex σ.

Fig. 14 shows the influence of the primary amplitude A on the subharmonic growth rate. The parameters involved are identical to those of Fig. 11b with $\beta_2 = 2.1$. We note that σ_r increases with A, and that the subharmonic modes are unstable only when A is larger than 1.2%

VI.2.3. Secondary Eigenfunctions

Our previous results indicate that the primary wave can trigger a strong growth of secondary disturbances. We proceed next to examine the influence of compressibility on the secondary eigenfunctions, which determine the structure of the secondary disturbance normal to the plate.

The fundamental eigenfunctions at $M_\infty = 1.6$ associated with wavenumbers $\alpha_2 = 0$ and $\alpha_2 = 0.24$ are displayed in Figs. 15a and 15b respectively. These eigenfunctions correspond to the dominant fundamental instability with a 2-d primary mode at $M_\infty = 1.6$ and $A = 1.5\%$. The results are obtained using $Re = 1675$, $T_\infty = 520^0$ R, $\alpha = 0.24$, $\beta = 0$, $\beta_2 = 0.4$, 45 grid points and 3 Fourier modes. The two most dominant components of the secondary eigenfunctions, in order of importance, are the streamwise velocity components $u_{2,0}$ and $u_{2,1}$. Both components peak near the critical point (i.e., $y \approx 1.0$). In contrast, at this Mach number, the strongest primary eigenfunction is the temperature component.

Fig. 15a shows that the y-distributions of the temperature, density and spanwise velocity eigenfunctions all have two local maxima across the boundary layer. A comparison with the corresponding incompressible case in Fig. 16a reveals two compressibility effects. First, at higher M_∞ the peaks of the eigenfunctions are pushed away (in dimensional units) from the wall. For example, while $u_{2,0}$ peaks near $y^* = 0.7\delta^*$ $(= y_0^*)$ at $M_\infty = 0$, it peaks near $y^* = 0.9\delta^*$ $(= y_1^*)$ at $M_\infty = 1.6$. Since $\delta^* = 2.72\sqrt{\nu_\infty^* x^*/u_\infty^*}$ at $M_\infty = 1.6$ and $\delta^* = 1.72\sqrt{\nu_\infty^* x^*/u_\infty^*}$ at $M_\infty = 0$, it is clear that y_1^* is about twice as large as y_0^* — recall that the superscript $*$ indicates a dimensional quantity. The second effect of compressibility is to make the spanwise velocity eigenfunction $w_{2,0}$ become insignificant relative to the streamwise velocity eigenfunction $u_{2,0}$.

Fig. 15b shows that the eigenfunctions (except for $u_{2,1}$) associated with $\alpha_2 = 0.24$ at $M_\infty = 1.6$ are characterized by a major peak across the boundary layer. The $|u_{2,1}|$ component has two peaks: one very small one at $y \approx 0.01$ (not clearly shown in the figure) and the other at $y \approx 0.9$.

Fig. 16b shows that although the velocity eigenfunctions at $M_\infty = 0$ are qualitatively similar to Fig. 15b, there are some noticeable differences. For example, the ratio of the maximum value of $|w_{2,1}|$ to the maximum value of $|u_{2,1}|$ is about 0.8 at $M_\infty = 0$, whereas this ratio becomes 0.5 at $M_\infty = 1.6$.

The influence of compressibility on the subharmonic eigenfunctions is examined at Mach numbers 0, 1.6 and 4.5, and is illustrated in Figs. 17-19. These figures show that compressibility introduces temperature and density fluctuations which become increasingly significant at higher Mach numbers. Since $\delta^*(= 10.5\sqrt{\nu^* x^*/u_\infty^*}$ at $M_\infty = 4.5)$ increases rapidly with increasing M_∞, the figures confirm that the vertical location (in dimensional unit) of the subharmonic perturbations peaks are pushed towards the free stream by increasing M_∞. Moreover, the eigenfunctions at $M_\infty = 4.5$ (centered near the critical point) are confined to a much narrower region than those at lower Mach numbers. Furthermore, although the streamwise velocity perturbation is the dominant perturbation at $M_\infty = 0$ and $M_\infty = 1.6$, the temperature perturbation becomes the largest one at $M_\infty = 4.5$.

VI.2.4. Reynolds number effect

We determine here the Reynolds number beyond which the inviscid secondary disturbance equations can capture the correct instability characteristics of secondary disturbances. To this effect, we vary the Reynolds number (only) in the secondary disturbance equations. A calculation is performed for the most amplified secondary disturbance at $M_\infty = 4.5$ and $A = 6\%$. The parameters are $T_\infty = 110^0 R, \alpha = 2.52, \beta = 0, e_h = 1, N = 2$, and $\beta_2 = 2.1$. The Reynolds number used for the primary mode is 1×10^4, while it ranges from 1×10^4 to 1.49×10^7 for the secondary mode. The results are shown in Fig. 20. We note that the second mode subharmonic is inviscid in character in the sense that σ_r increases (monotonically) with Re and asymptotes to an inviscid limit. The figure demonstrates that inviscid results can be obtained from the viscous problem in the limit of vanishing viscosity. However, the growth rate of the subharmonic can be obtained within 1% accuracy from inviscid calculations only for Reynolds numbers higher than a million. For example, σ_r at $Re = 1 \times 10^4$ is only about 45% of the inviscid growth rate.

The corresponding effects of Reynolds number on the subharmonic eigenfunctions are depicted in Figs. 19, 21 and 22. While the viscosity minimally affects the thermodynamic variables $t_{2,1}$ and $\rho_{2,1}$ (which are the dominant perturbations), it plays an appreciable diffusive role on the streamwise velocity eigenfunction ($u_{2,1}$) and the the spanwise velocity eigenfunction ($w_{2,1}$).

VI.2.5. Primary wave angle effect

Recall that the most unstable primary disturbance in supersonic and hypersonic flows can be oblique (with respect to the mean flow direction). The influence of the primary wave angle θ on σ_r is examined at $M_\infty = 1.6$, $Re = 1675$, $T_\infty = 520^0 R$, $\alpha = 0.24$, and $A = 1.5\%$. First small to moderate values of θ are examined for $\theta = 0^0, 5^0, 10^0, 15^0$. The primary modes are slightly unstable with growth rates varying from 3.7×10^{-5} at $\theta = 0$ to 1.42×10^{-3} at $\theta = 45^0$. Since the secondary instabilities of a 2-d primary wave can be accurately determined using the lowest order of approximation defined by Eqs. 27-28, we *assume* that this approximation will not incur significant errors in the determination of σ for the aforementioned values of θ; consequently, the convergence of σ in terms of the Fourier modes is not verified. In Figs. 23-24, σ_r is plotted against β_2. It is found that when $\theta \neq 0^0$, the secondary disturbances do not travel with the phase velocity of the primary disturbance. The figures show that while the strongest subharmonic mode occurs when the primary disturbance propagates in the mean flow direction, the most unstable fundamental mode occurs when $\theta \approx 10^0$. When $\theta \geq 10^0$, there are two local maxima in the curve of σ_r versus β_2. Because the second maximum is relatively smaller than the first maximum, it will probably have no significant impact on boundary-layer transition. It is also worth noting that the growth rates of the unstable waves with small β_2 are only very weakly dependent on the orientation of the primary wave, especially for small values of θ. Since neither the largest primary growth rate nor the largest fundamental growth rate corresponds to a 2-d primary, it is inappropriate to examine the fundamental instability based on a 2-d primary wave, at least at $M_\infty = 1.6$.

It is known that at $M_\infty = 1.6$, the most unstable primary wave occurs at $\theta = 45^0$. Since this value of θ is appreciably high, it is appropriate to first perform convergence studies of the effect of the higher fourier modes on secondary instabilities. The results, together with the corresponding case for $\theta = 0^0$, are illustrated in Table 5.

Subharmonic modes	Number of Fourier Modes	65 points	
		$10^2\ \sigma_r$	$10^2\ \sigma_i$
$\theta = 0^0$	2	1.201	0
	3	1.209	0.003
	4	1.216	0
	5	1.216	0
$\theta = 45^0$	2	0.316	10.415
	3	1.078	10.534
	4	1.078	10.534
	5	1.123	10.527
	6	1.123	10.527

Table 5

We see that when the primary is 2-d, the first two Fourier modes can capture σ correctly to 3 decimal places. However, when $\theta = 45^0$, the first two Fourier modes are *not sufficient* to accurately determine σ. The first 3 Fourier modes determine σ correctly to 2 decimal places. The results from Table 5 can easily be explained by the corresponding eigenfunctions. The normalized streamwise velocity eigenfunctions, which are the most dominant components, are shown in Fig. 25 for $\theta = 0^0$ and Fig. 26 for $\theta = 45^0$. When $\theta = 0^0$, the eigenfunctions associated with $\alpha_2 = \pm\tilde{\alpha}/2$ are the most important components, while those associated with higher values of α_2 are increasingly negligible. Consequently, σ can be accurately determined by using only the first two Fourier modes. When $\theta = 45^0$, the eigenfunctions associated with $\alpha_2 = \tilde{\alpha}/2$ and $\alpha_2 = 3\tilde{\alpha}/2$ are respectively the two most important components. Other eigenfunctions are relatively insignificant. Therefore, σ can be determined with sufficient accuracy using the modes $\alpha_2 = \tilde{\alpha}/2$ and $\alpha_2 = 3\tilde{\alpha}/2$, but not using the components with $\alpha_2 = \pm\tilde{\alpha}/2$. Finally, it is interesting to note that the eigenfunctions with $\alpha_2 = -3\tilde{\alpha}/2$ is practically negligible. This explains why σ does not change when N is increased from $N = 3$ to $N = 4$ in Table 5. Hence, caution must be taken when performing the convergence studies on the eigenvalue σ.

VII. Conclusions

A fully spectral code has been developed to study the linear secondary instabilities of compressible boundary layers on insulated flat plates. This code, which allows 2-d or 3-d primary disturbances and an arbitrary number of secondary modes of different types, has been verified against existing data for incompressible boundary layers and against direct numerical simulations at $M_\infty = 1.6$ and 4.5.

The influence of the (2-d) primary mode amplitude A on the secondary instability characteristics has been studied at four Mach numbers: $M_\infty = 0, 0.8, 1.6, 4.5$. We found that a small but finite primary disturbance amplitude can trigger a broad-band of highly unstable 3-d secondary disturbances whose growth rates are large and increase with increasing A. Increasing the free stream Mach number not only pushes the disturbances away from the wall, but also confines them to a much smaller region, centered near the critical point.

The influence of the primary disturbance skewness θ (with respect to the mean flow direction) on secondary instability characteristics at $M_\infty = 1.6$ is first examined for $\theta = 0^0, 5^0, 10^0, 15^0$. The unstable subharmonic and the fundamental disturbances propagate with the same phase velocity as the 2-d primary, whereas their phase velocities are different from the phase velocity of the 3-d primary. For $\theta = 10^0$ and $\theta = 15^0$, there are two maxima in the curve of the growth rate, σ_r, versus the wavenumber in the direction parallel to the phase front of the primary wave (i.e., β_2). The strongest subharmonic modes occur when the primary disturbance propagates in the mean flow direction, while the most unstable fundamental modes occur when the primary disturbance is inclined at about 10^0 to the mean flow direction. When the subharmonic instability is examined at a relatively high value of θ (namely, $\theta = 45^0$), it is found the first five Fourier modes (i.e. $N = 5$) are required to capture the secondary growth rate correctly to 4 significant digits.

At $M_\infty = 4.5$, there are two types of primary instability modes: first and second mode. At this Mach number, the subharmonic and fundamental instabilities which originate from both the first and the second mode waves are examined. We found that the subharmonic instabilities which arise from the second mode disturbances are the dominant instabilities. When the primary wave amplitude increases from 2 % to 6 %, the growth rate of the most amplified subharmonic of a second mode disturbance is augmented by about 136%.

In summary, we believe that secondary instability is a viable boundary-layer transition mechanism at $M_\infty = 0.8, 1.6$ and 4.5. Further, the high frequency, acoustic type second mode subharmonic (secondary) disturbances will prevail at $M_\infty = 4.5$.

VIII. Acknowledgments

The authors would like to thank Drs. Thomas Zang and Craig Streett for their numerous suggestions. Dr. Dave Pruett's assistance in validating the stability theory with direct numerical simulations is greatly appreciated. The first author was supported by NASA Langley Research Center under contracts NAS1-18599.

References

[1] Bushnell, D., and Malik, M. 1985: Application of Stability Theory to Laminar Flow Control — Progress and Requirements. *In Stability of Time Dependent and Spatially Varying Flows,* ed. D. L. Dwoyer and M. Y. Hussaini, 1985 43-57.

[2] Crouch, J. D. 1988, " The nonlinear evolution of secondary instabilities in boundary layers," Ph.D. Thesis, VPI & SU.

[3] Erlebacher, G. and Hussaini, M. Y. 1987: Stability and Transition in Supersonic Boundary Layer. *AIAA Paper,* **87-1416**.

[4] Erlebacher, G. and Hussaini, M. Y. 1989: Numerical experiments in supersonic boundary-layer stability. *Phys. Fluids A,* Vol. **2**, No. **1**, 94-104.

[5] Gaster, M. 1962 "A note on the relation between temporally-increasing and spatially-increasing disturbances in hydrodynamic stability," *J. Fluid Mech.*, Vol. 14, 222-224.

[6] El Hady, N. M. 1989: Secondary Instability of Compressible Boundary Layer To Subharmonic Three-Dimensional Disturbances. *AIAA Paper,* **89-0035**.

[7] Herbert, T., Bertolotti, F.and Santos, G. 1985: Floquet Analysis of Secondary Instability in Shear Flows. *In Stability of Time Dependent and Spatially Varying Flows,* ed. D. L. Dwoyer and M. Y. Hussaini, 1985 43-57.

[8] Lees, L. and Lin, C. C. 1946: Investigation of the Stability of the Laminar Boundary Boundary Layer in Compressible Fluid. NACA Tech. Note No. **1115**.

[9] Malik, M. R. 1989: Prediction and control of Transition in Supersonic and Hypersonic Boundary Layers. *AIAA Journal,* **27**, no. 11.

[10] Mack, L. M., 1969: Boundary-Layer Stability Theory. *Document 900-277, Rev. A, Jet Propulsion Lab., Pasadena, CA.*

[11] Nayfeh, A. H., 1989: NASA Conf. Proc. 3020 **1**, 629.

[12] Ng, L., Singer, B. Henningson, D. and Alfredsson, P. 1989: Instabilities In Rotating Channel Flow. *Proceedings of the Instabilities and Transition Workshop at NASA LARC,* May-June, 1990.

[13] Ragab, S. A. and Wu, J. L. 1990: Instabilities of Supersonic Flows. *AIAA Paper,* **90-0712**.

[14] Santos, German R. 1987: Studies on Secondary Instabilities. VPI & SU, Ph. D. Thesis.

[15] Streett, C. , Zang, T. and Hussaini, M. Y. 1984: Spectral methods for solution of the boundary-layer equation. *AIAA Paper,* **84-0170**.

[16] Wilkinson, J. H. 1965: *The algebraic Eigenvalue Problem.* Oxford University Press, London.

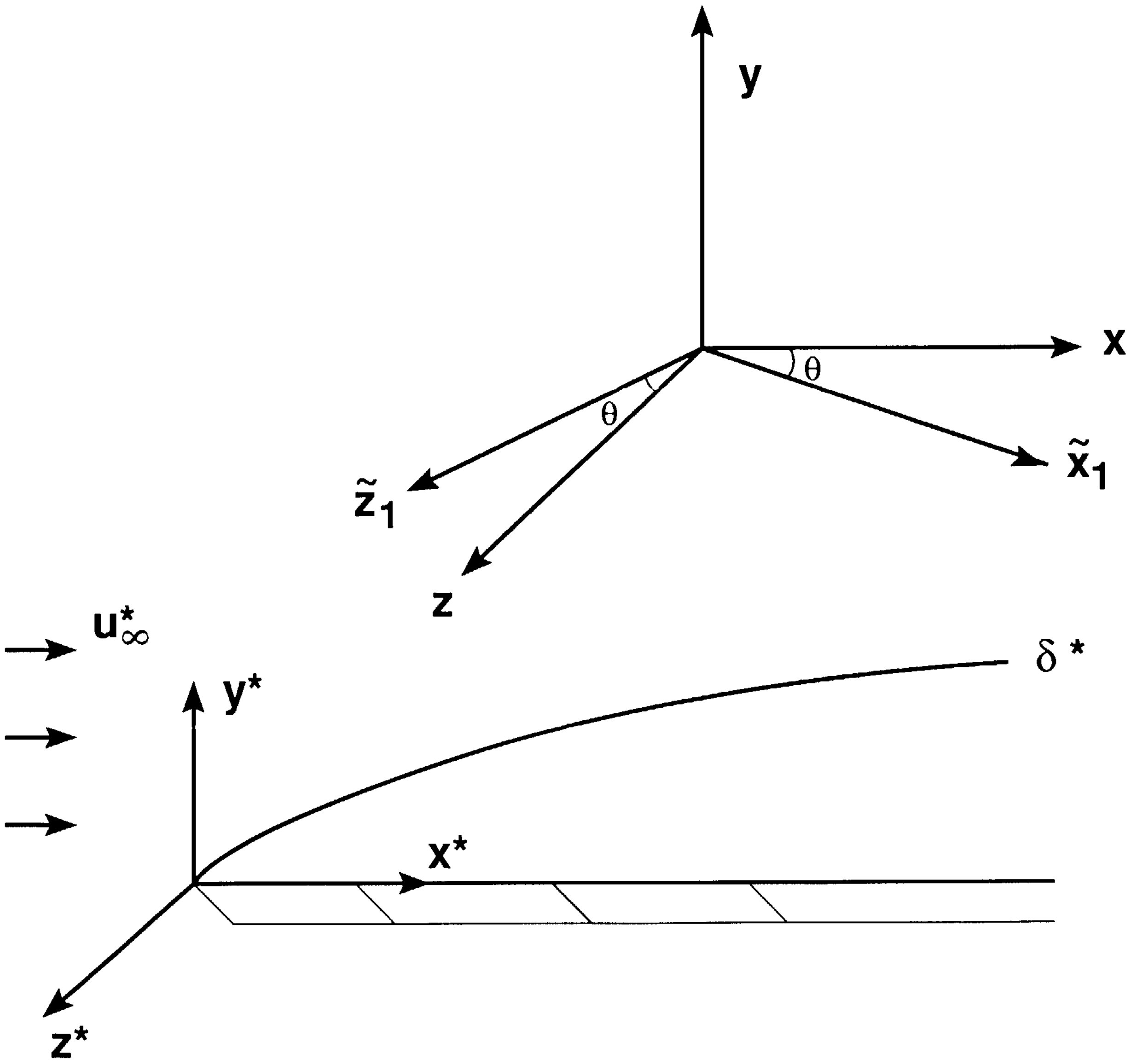
y
x
θ
θ
$\tilde{x}_1$
$\tilde{z}_1$
z
u^*_∞
y^*
x^*
δ^*
z^*

Fig.1: Schematic of boundary layer flows with definitions of coordinates.

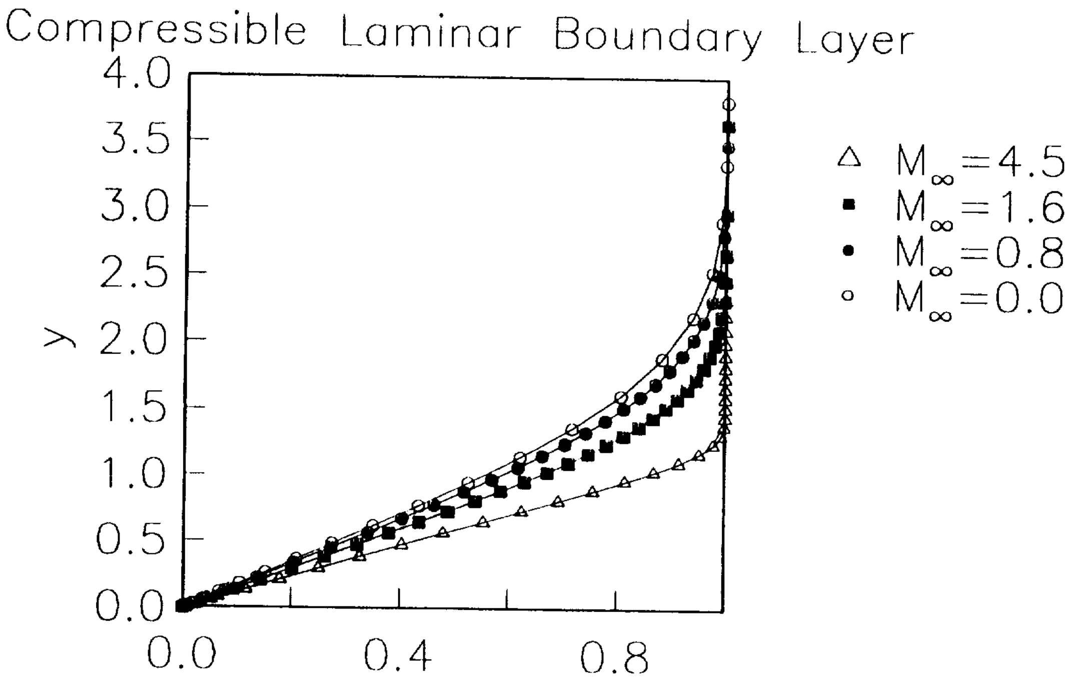

(a) mean velocity, u_0

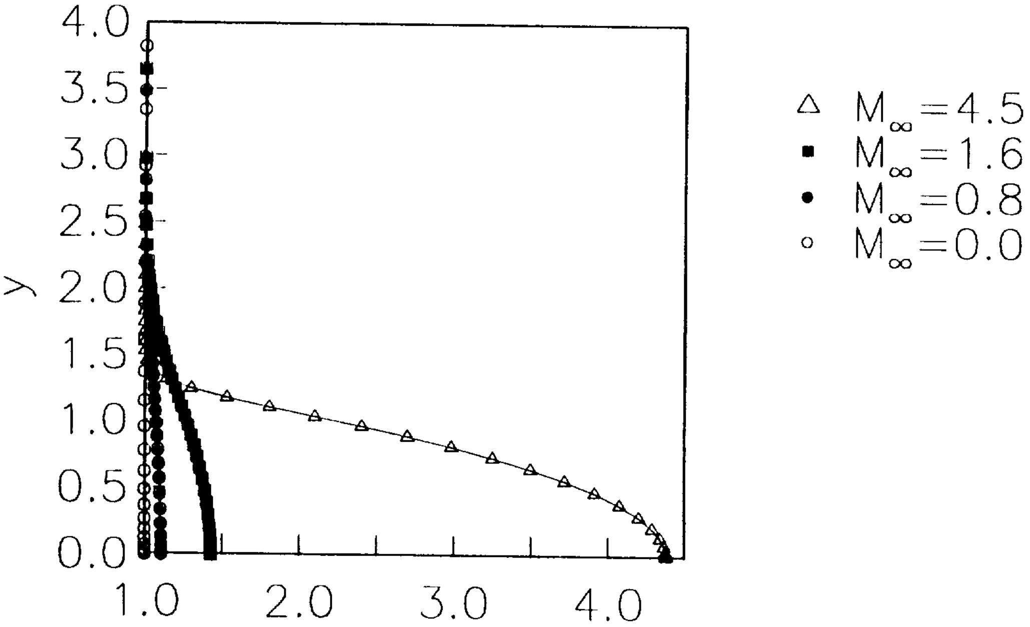

(b) mean temperature, T_0

Fig.2: Mean profiles for various Mach numbers. (a) mean velocity, (b) mean temperature.

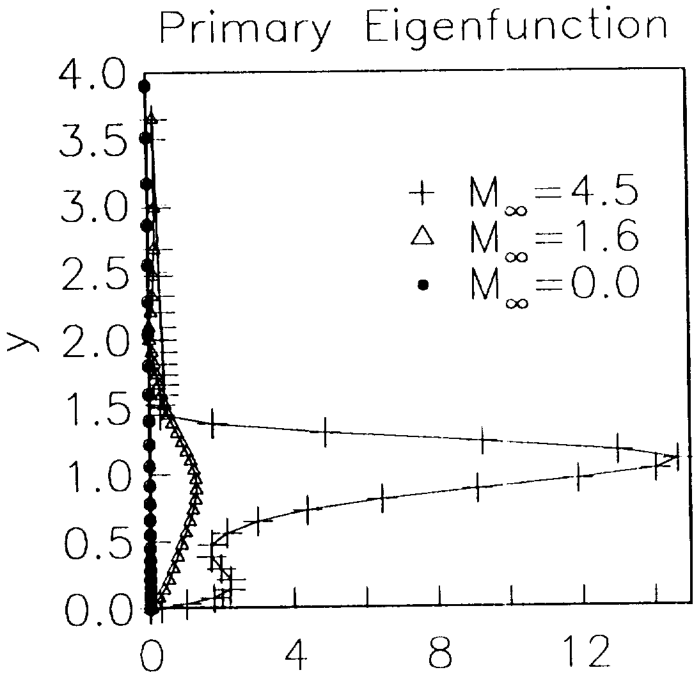

(a) $|\hat{T}_1|$

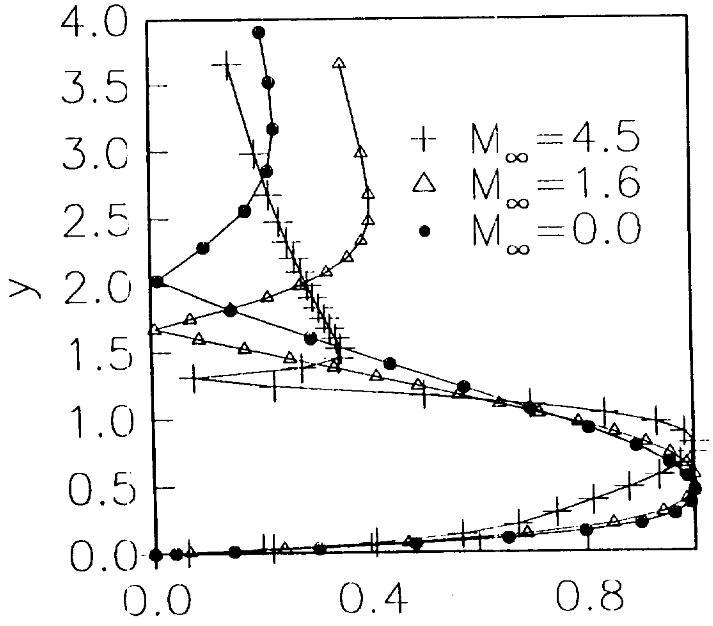

(b) $|\hat{u}_1|$

Fig.3: First mode 2-d eigenfunctions for various Mach numbers. $M_\infty = 0.0$, $\alpha = 0.29$, $Re = 1675$, $T_\infty = 520$. $M_\infty = 1.6, \alpha = 0.24, Re = 1675, T_\infty = 520$. $M_\infty = 4.5, \alpha = 0.6, Re = 10000, T_\infty = 110$.

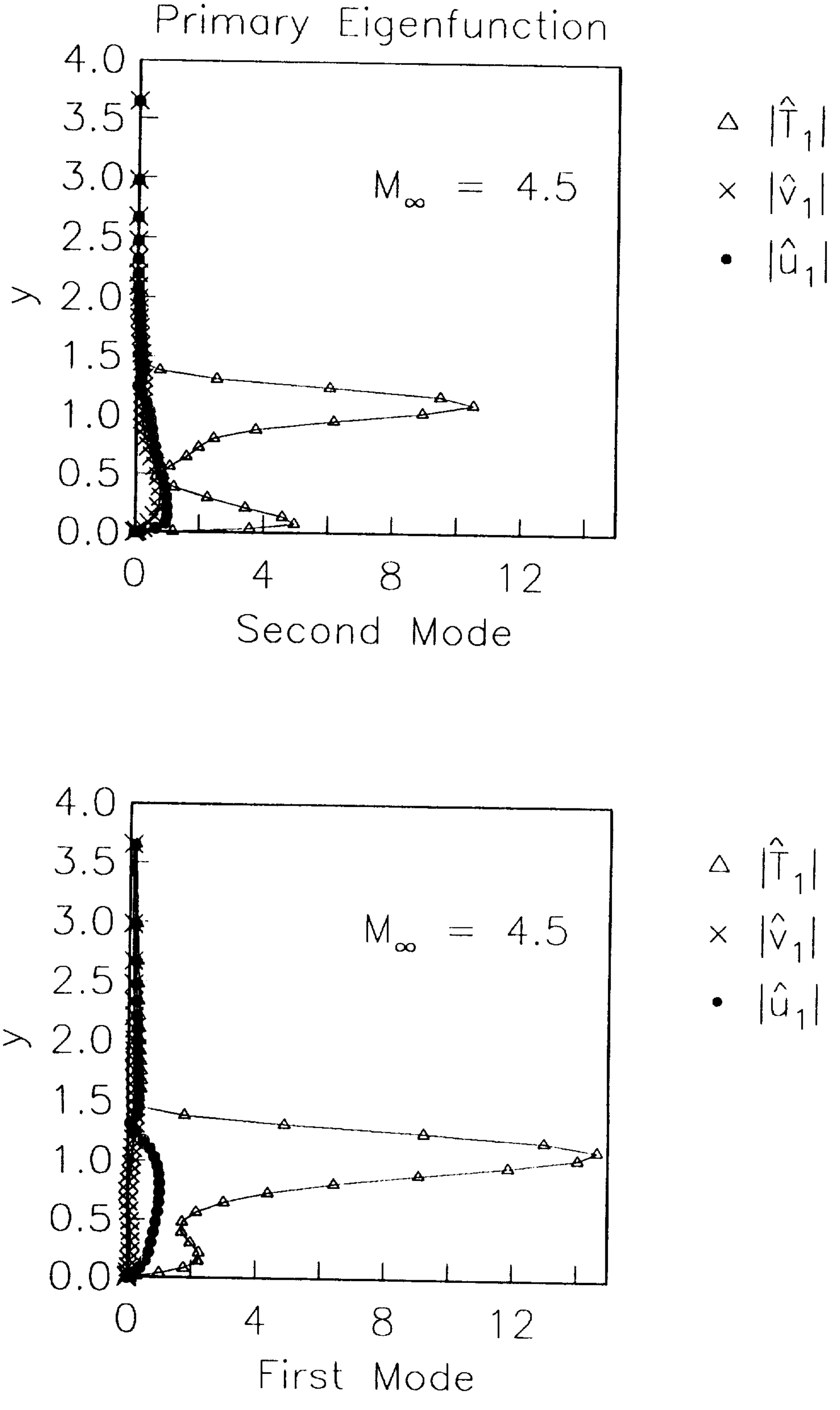

Fig.4: First mode and Second mode 2-d eigenfunctions at $M_\infty = 4.5$, $T_\infty = 110^0 R$ and $Re = 10000$. (a) First mode at $\alpha = 0.6$ (b) Second Mode at $\alpha = 2.25$.

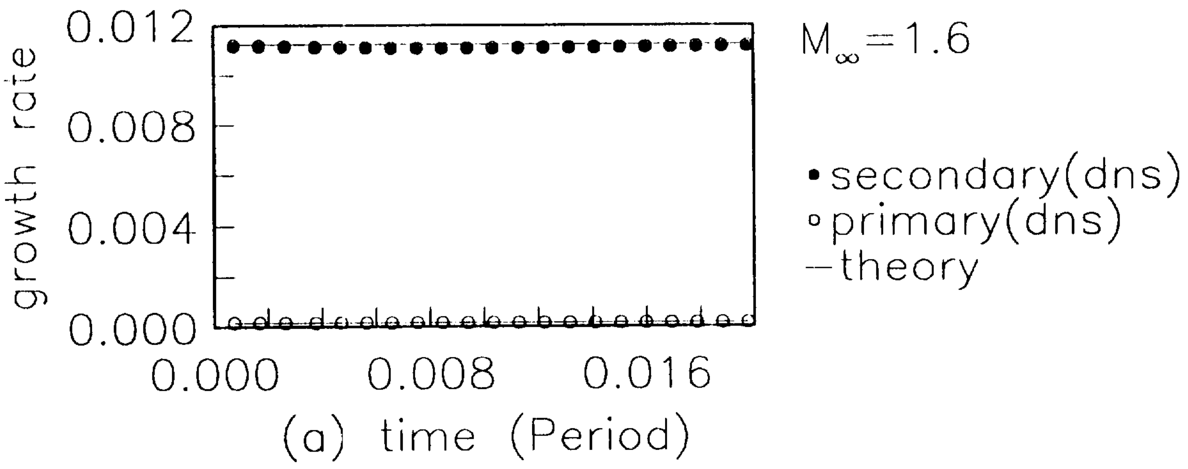

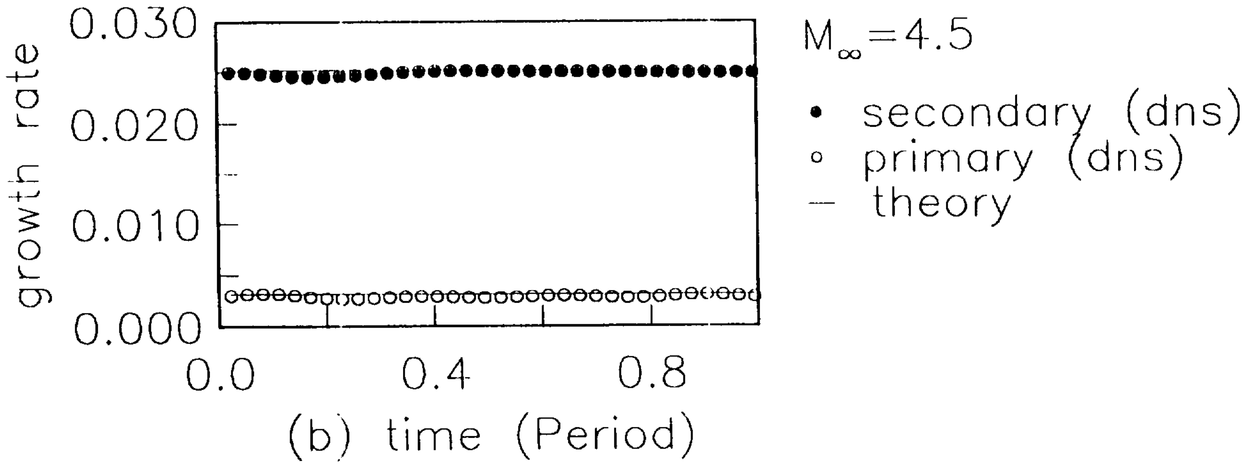

Fig.5: Comparison of theory with direct numerical simulation.

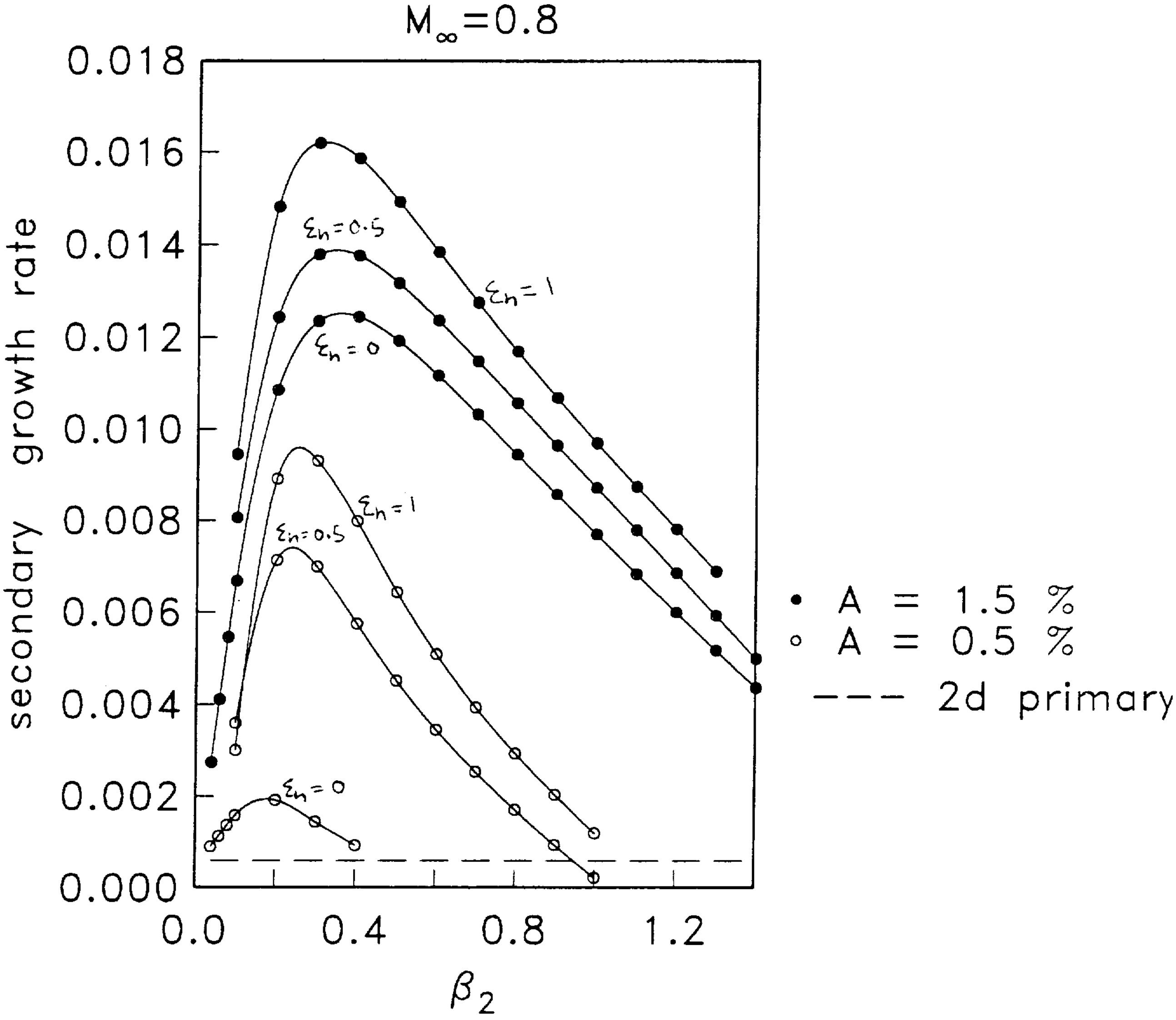

Fig.6: Secondary instabilities at $M_\infty = 0.8$. - - - primary growth rate.

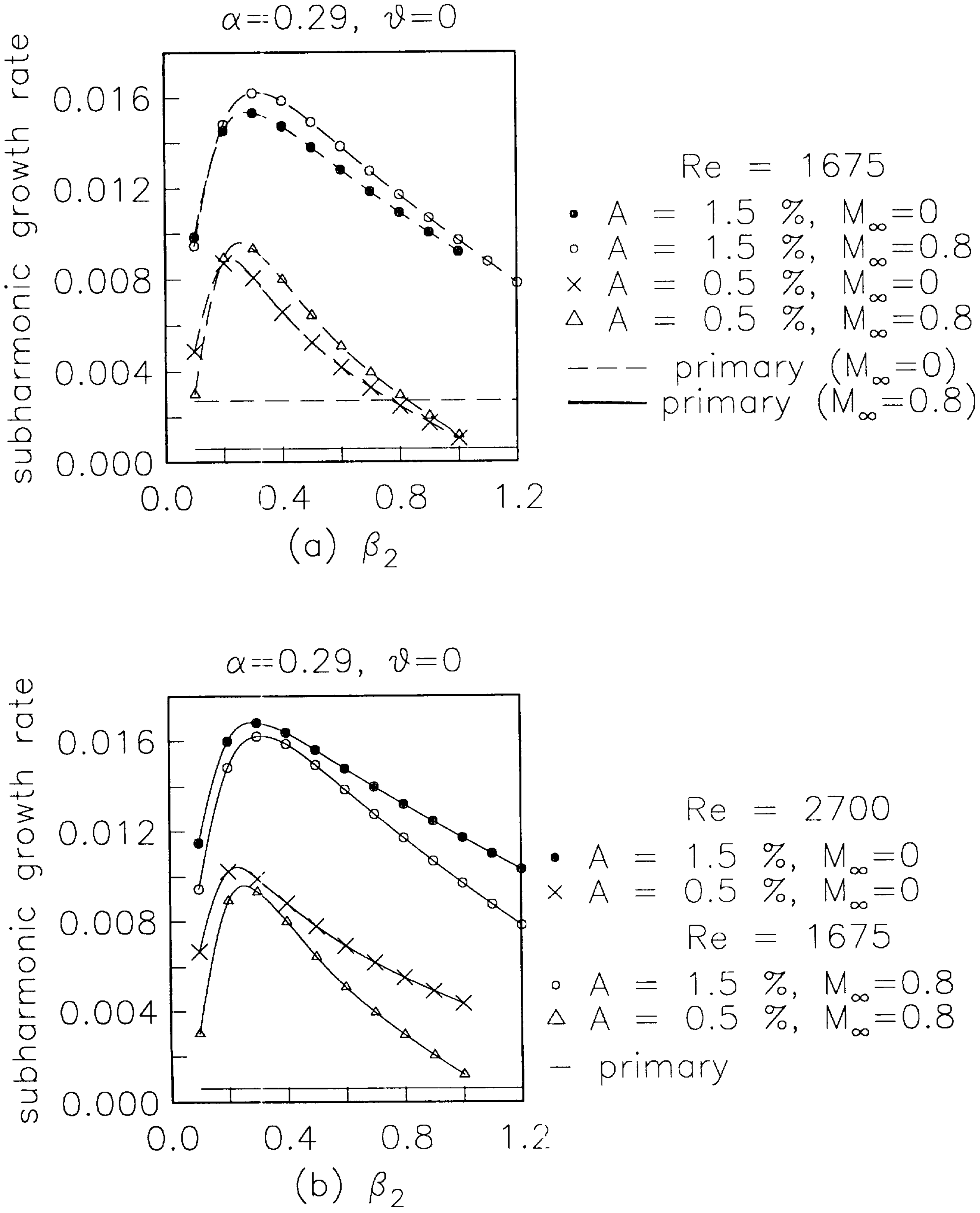

Fig.7: Comparisons between the subharmonic growth rates at $M_\infty = 0.0$ and $M_\infty = 0.8$.

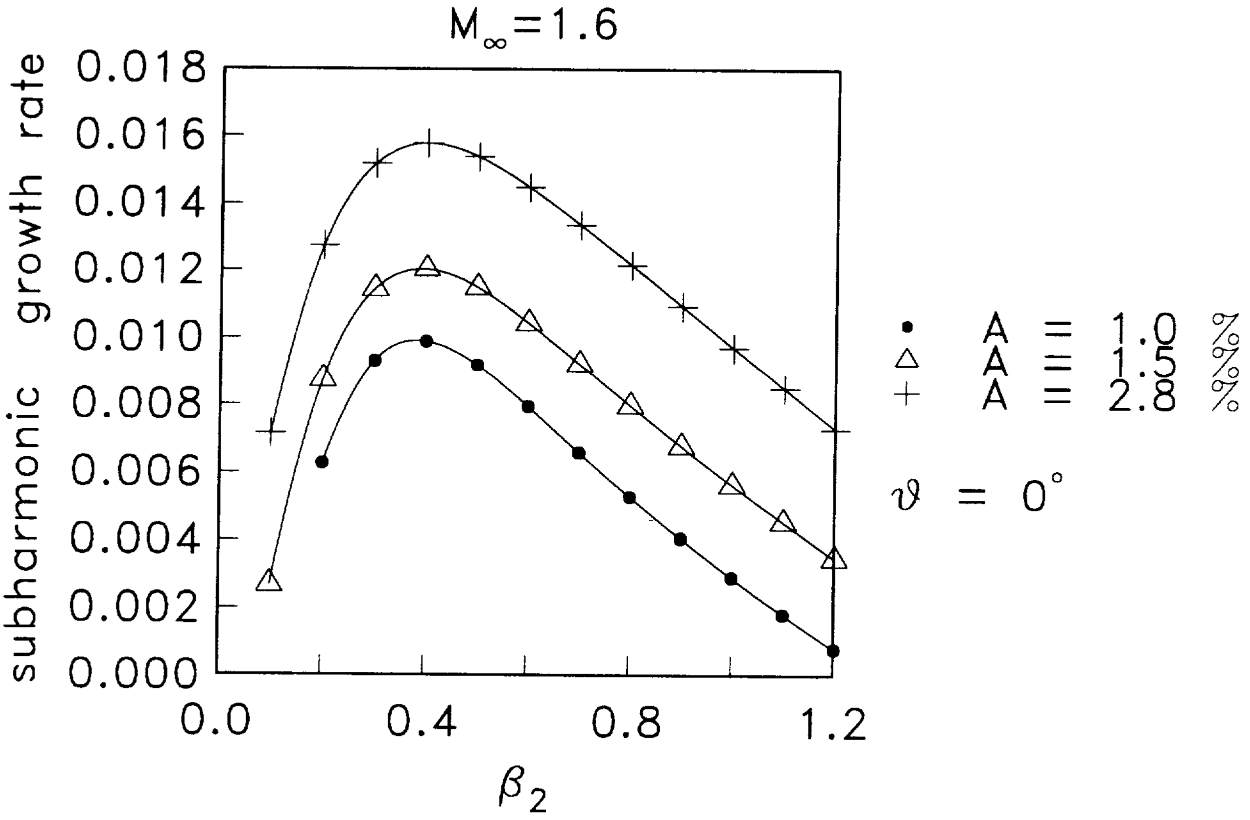

Fig.8: Subharmonic instabilities at $M_\infty = 1.6$. $\beta = 0$ and various A.

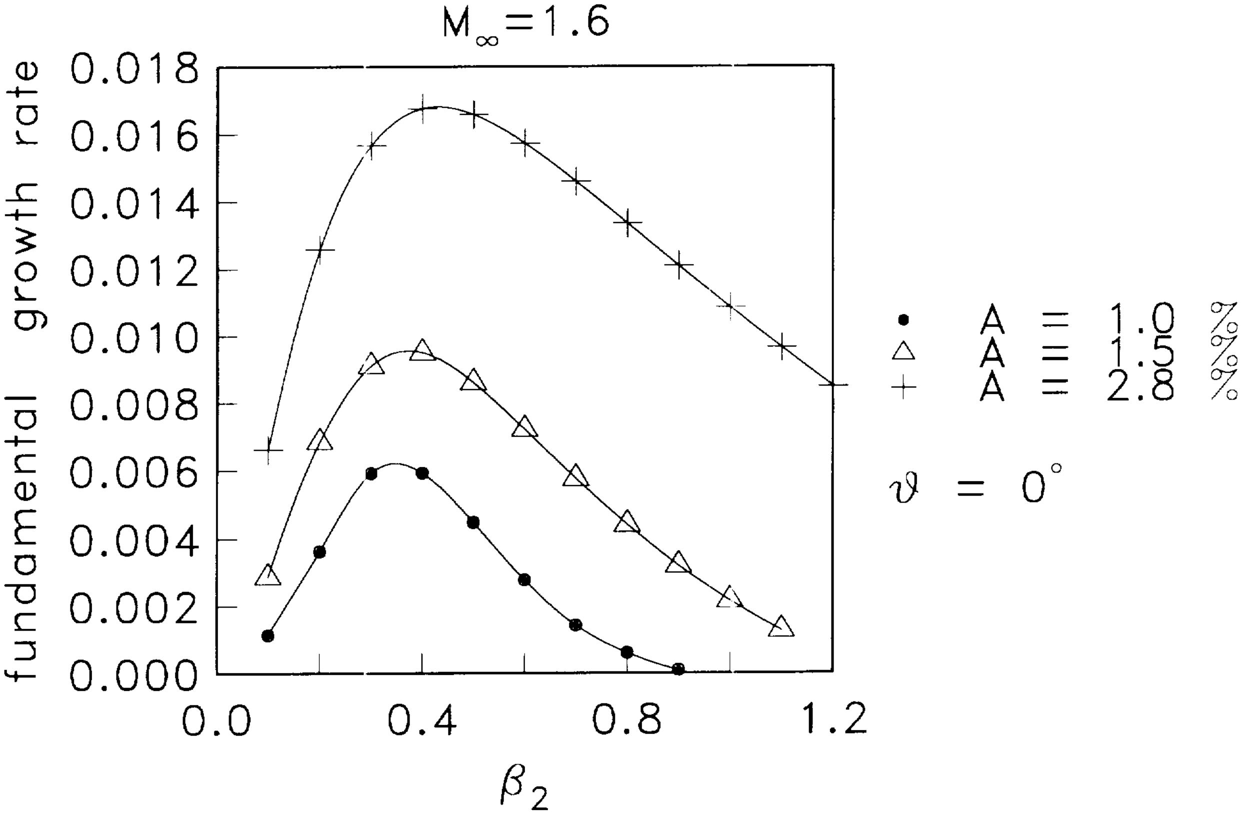

Fig.9: Fundamental instabilities at $M_\infty = 1.6$. $\beta = 0$ and various A,

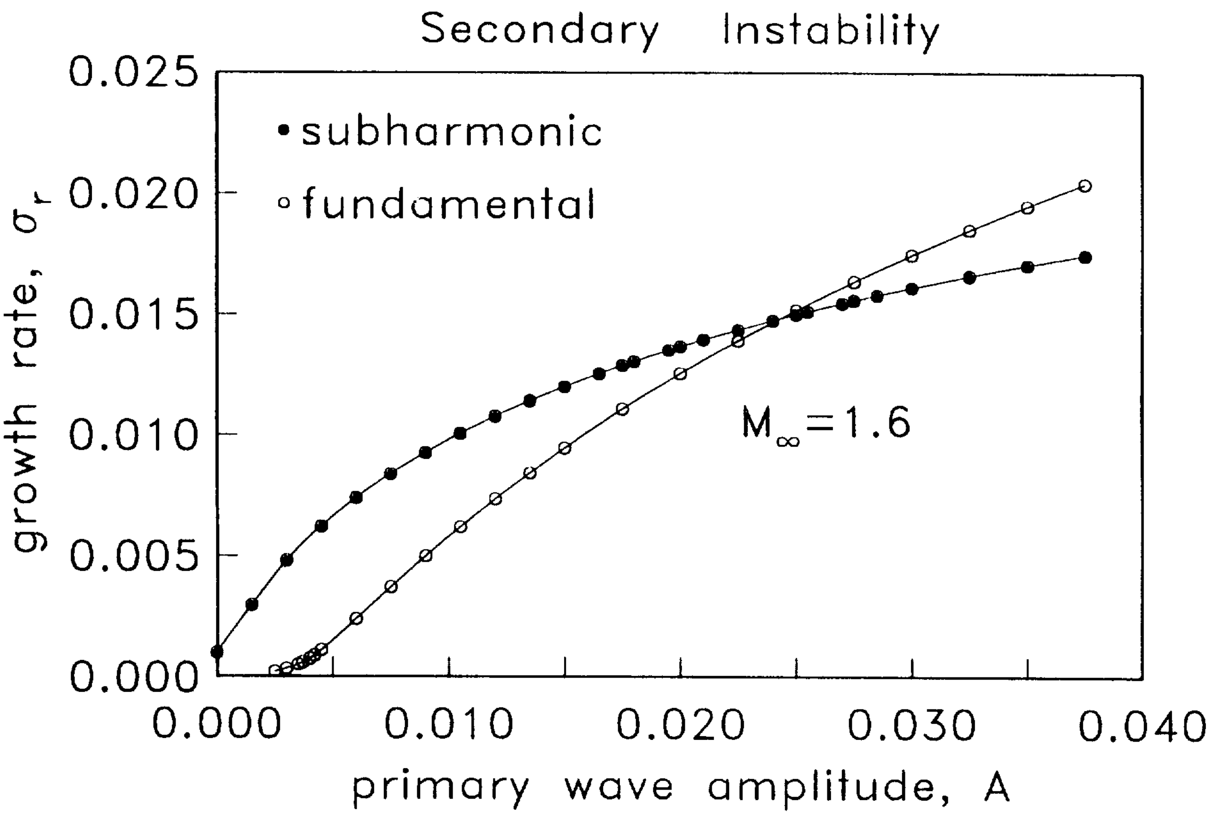

Fig.10: Growth rate as a function of primary wave amplitude. The results are for $M_\infty = 1.6, \alpha = 0.24$, $\beta = 0, \beta_2 = 0.4$, $T_\infty = 520^0 R$ and $Re = 1675$.

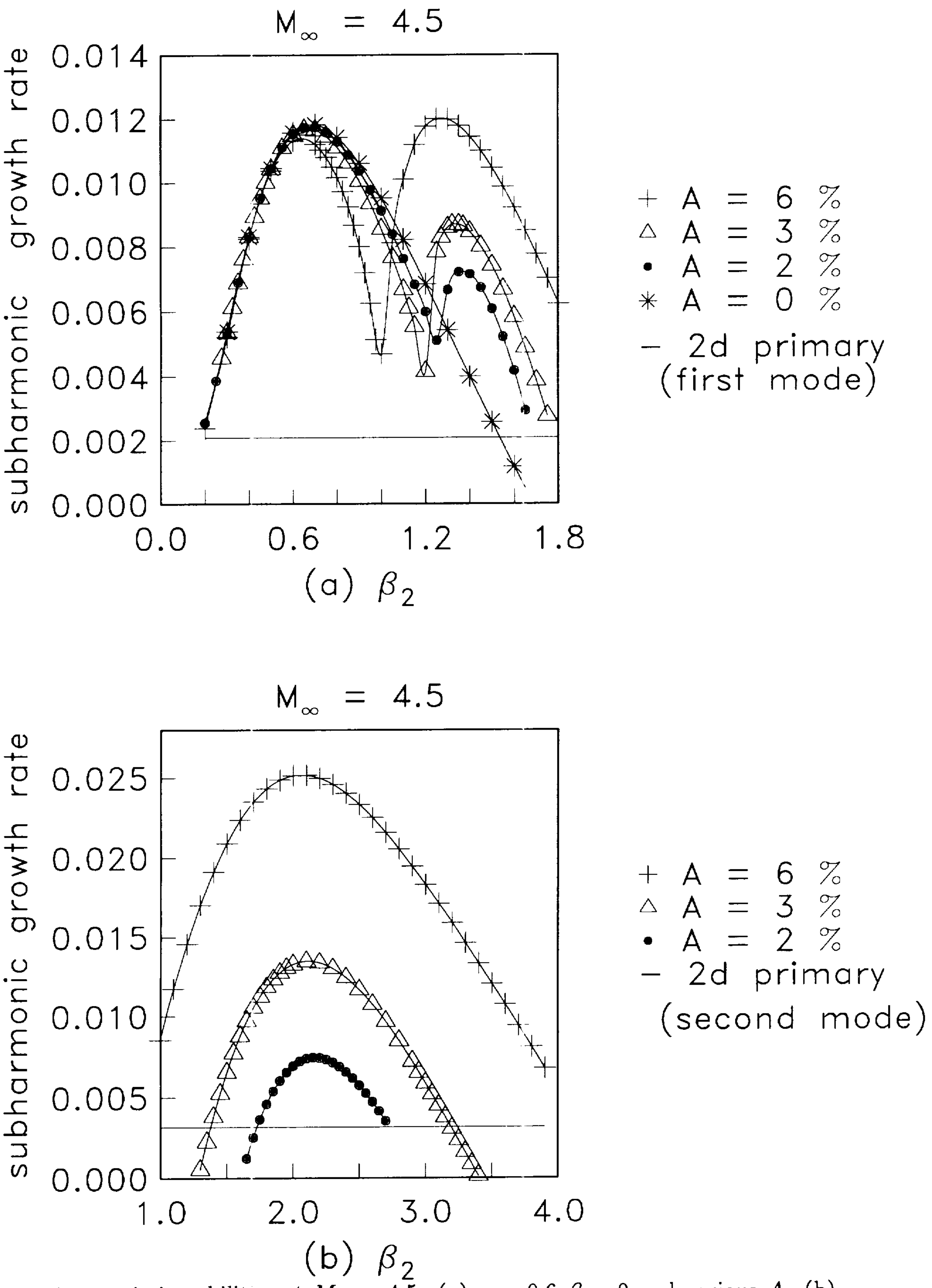

Fig.11: Subharmonic instabilities at $M_\infty = 4.5$. (a) $\alpha = 0.6, \beta = 0$ and various A. (b) $\alpha = 2.52, \beta = 0$ and various A. —— primary growth rate.

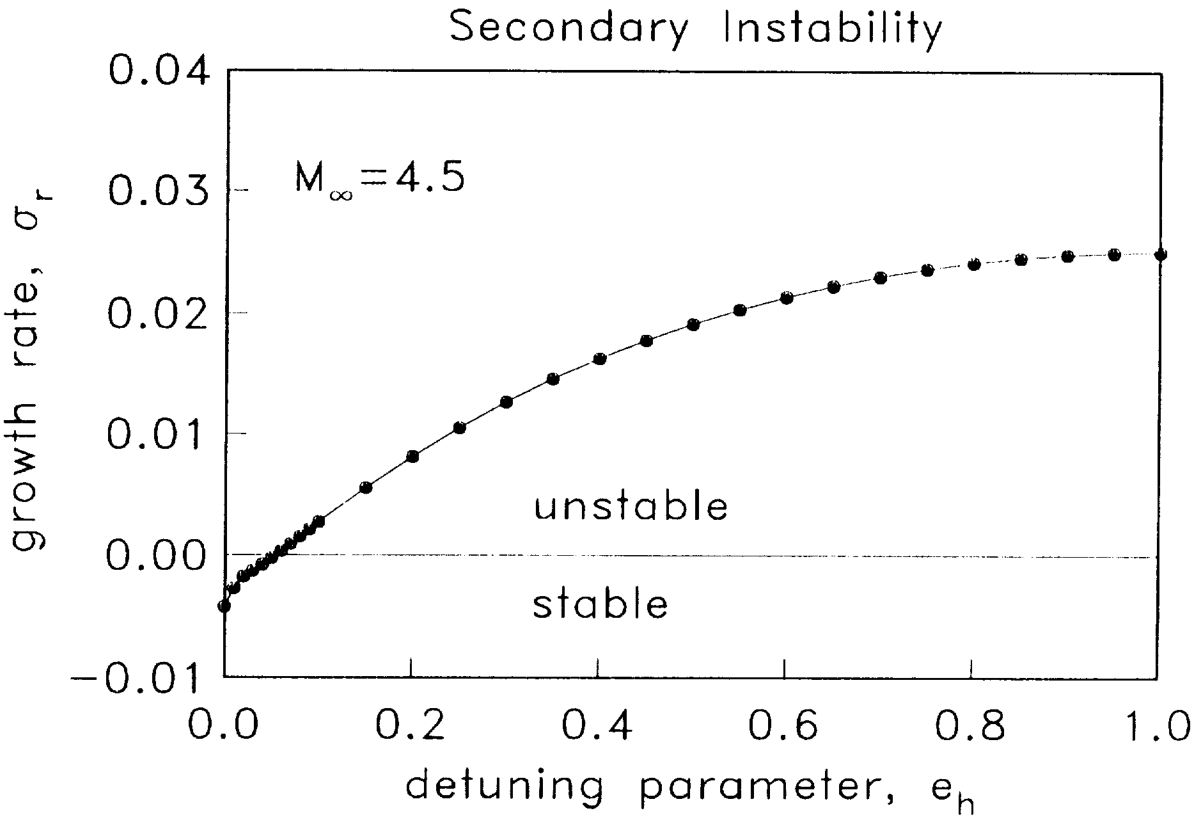

Fig.12: Growth rate as a function of the detuning parameter at $M_\infty = 4.5$.

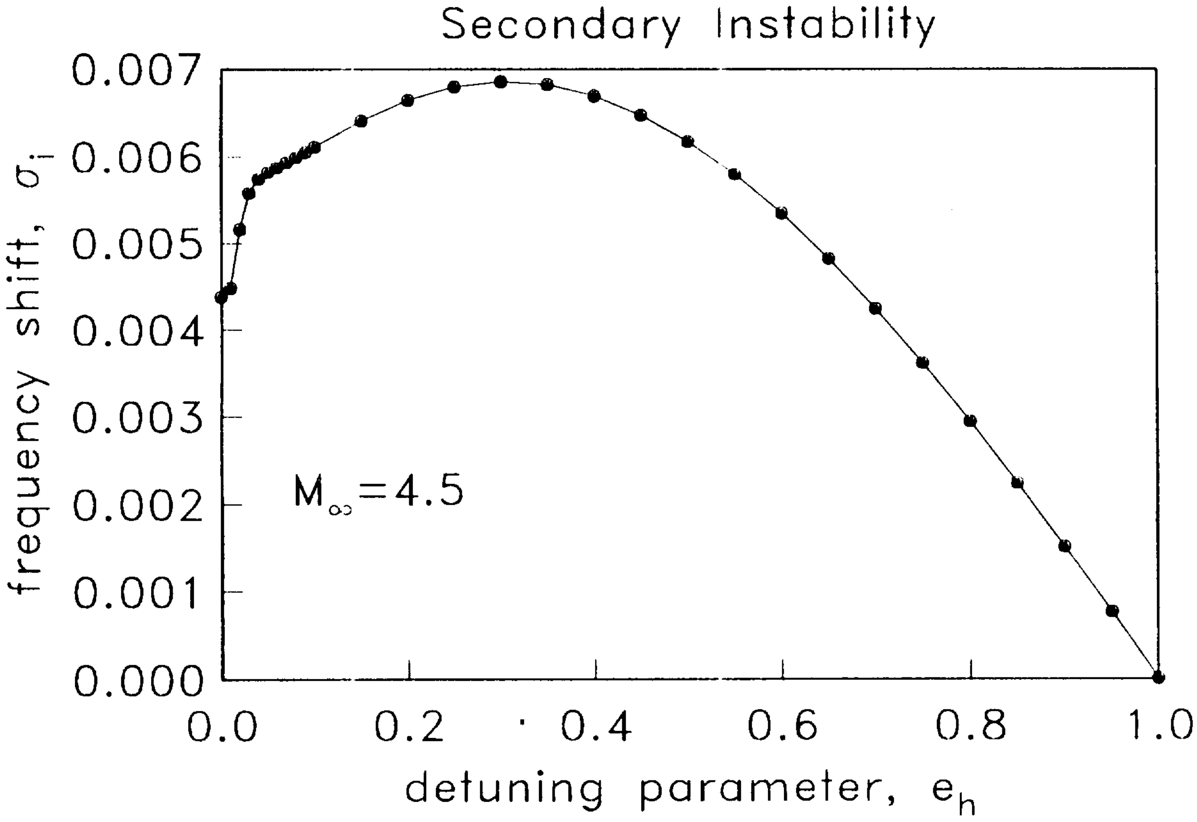

Fig.13: Frequency shift as a function of the detuning parameter at $M_\infty = 4.5$.

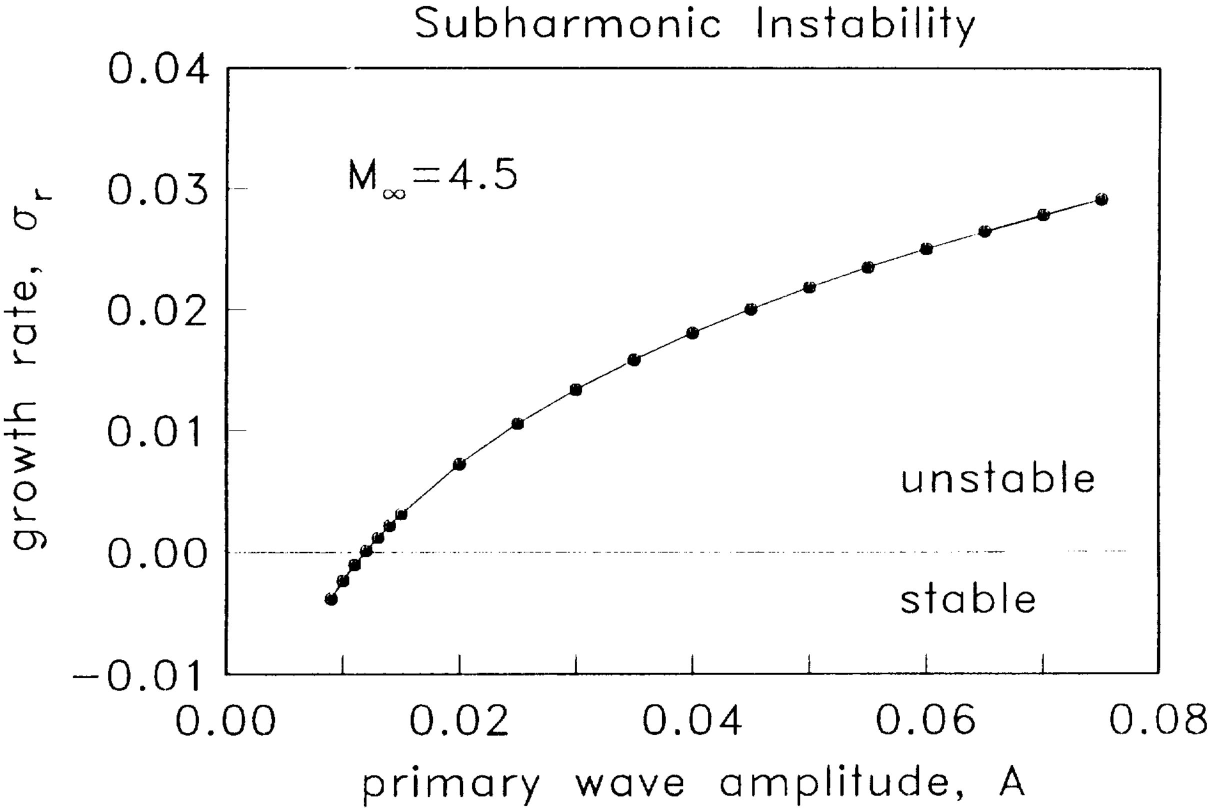

Fig.14: Subharmonic growth rate as a function of the primary wave amplitude at $M_\infty =$ 4.5. The results are for $\alpha = 2.52$, $\beta = 0$, $\beta_2 = 2.1$, $T_\infty = 110^0 R$, and $Re = 10000$.

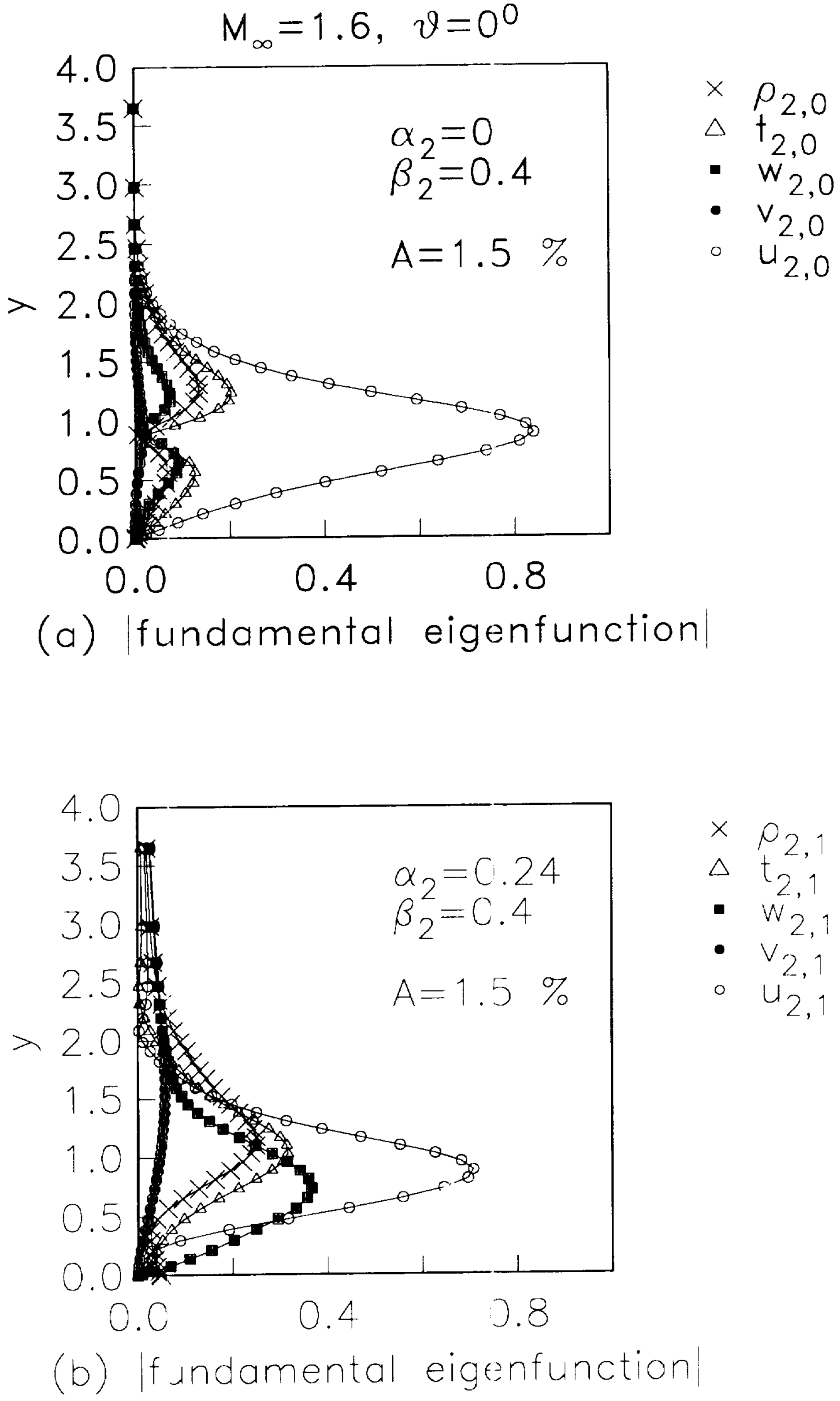

Fig.15: Fundamental eigenfunction at $M_\infty = 1.6$. Components of the eigenfunction with (a) $\alpha_2 = 0$ (b) $\alpha_2 = 0.24$.

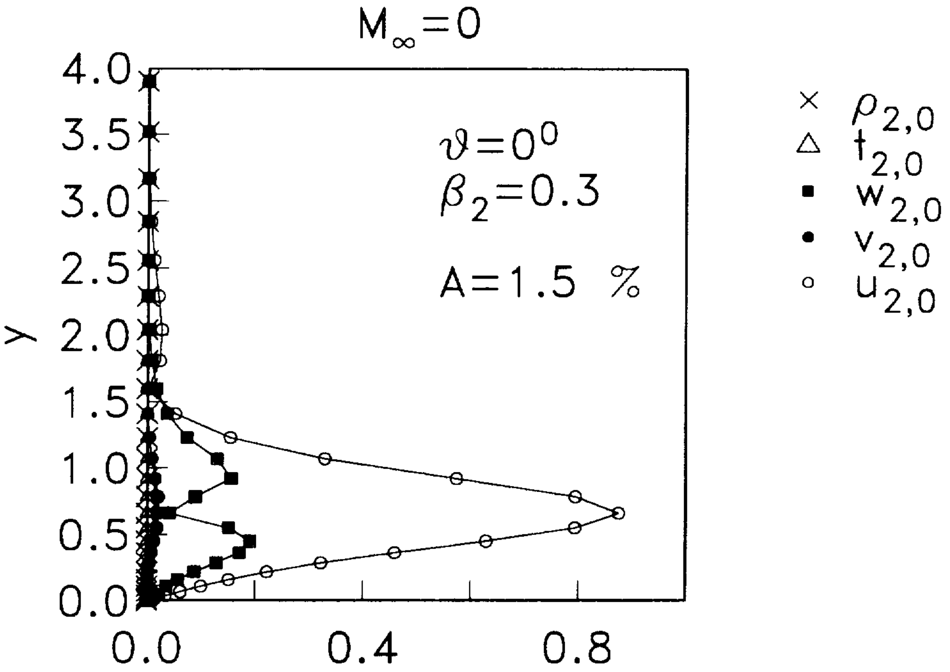

(a) |fundamental eigenfunction|

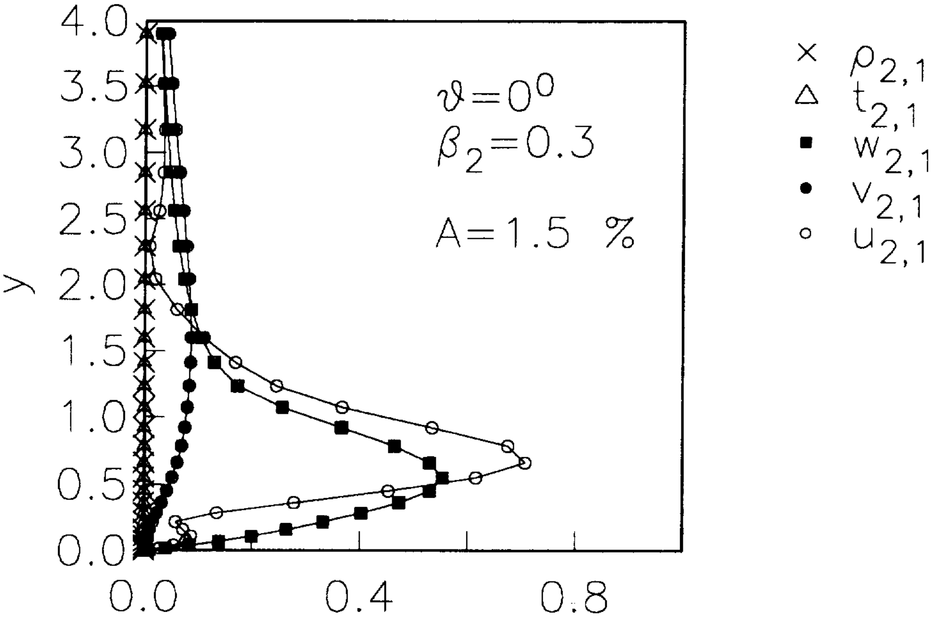

(b) |fundamental eigenfunction|

Fig.16: Fundamental eigenfunction at $M_\infty = 0.0$, $\alpha = 0.29$, $\beta = 0$, $T_\infty = 520^0R$, $Re = 1675$, and $A = 1.5\%$. Components of the eigenfunction with (a) $\alpha_2 = 0$. (b) $\alpha_2 = 0.29$.

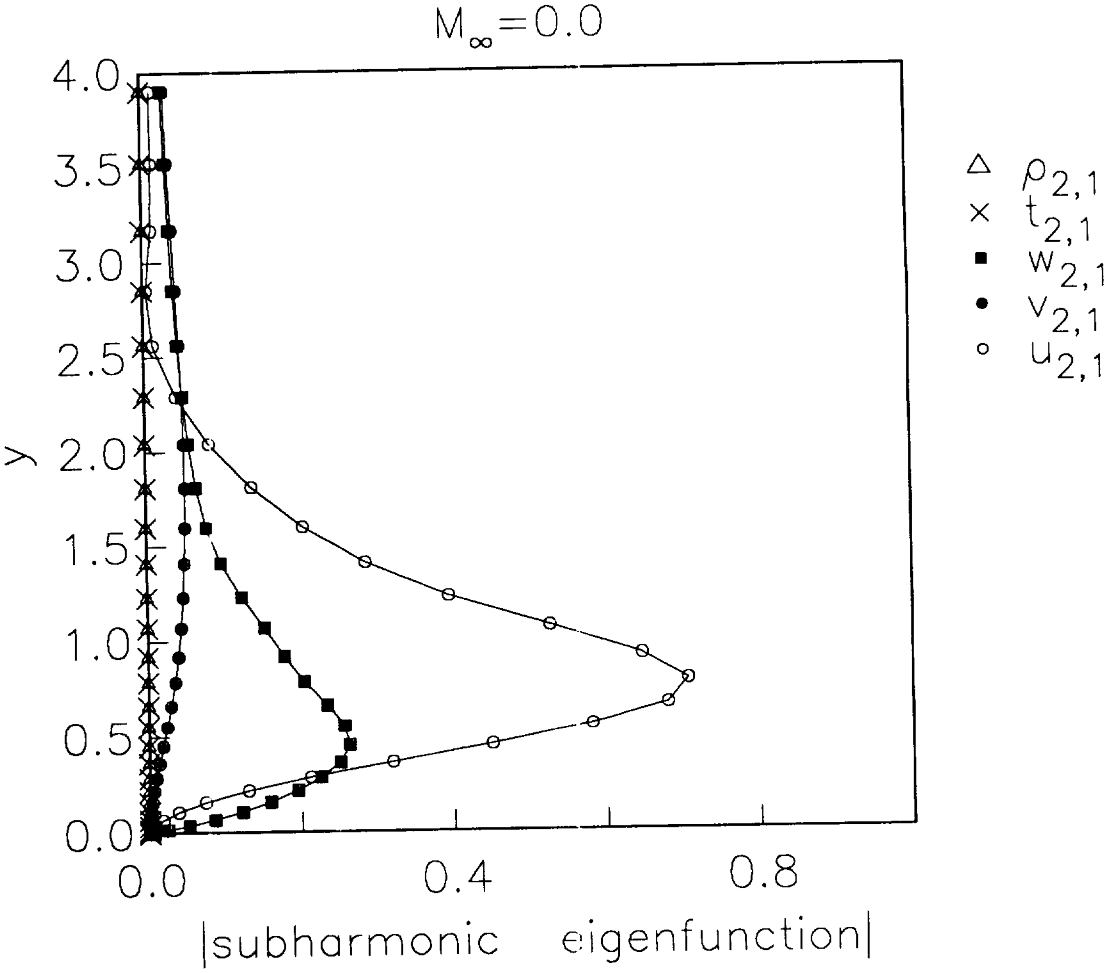

Fig.17: Subharmonic eigenfunction at $M_\infty = 0.0$. The parameters are $\alpha = 0.29$, $\theta = 0^0$, $T_\infty = 520^0R$, $Re = 1675$, and $A = 1.5\%$.

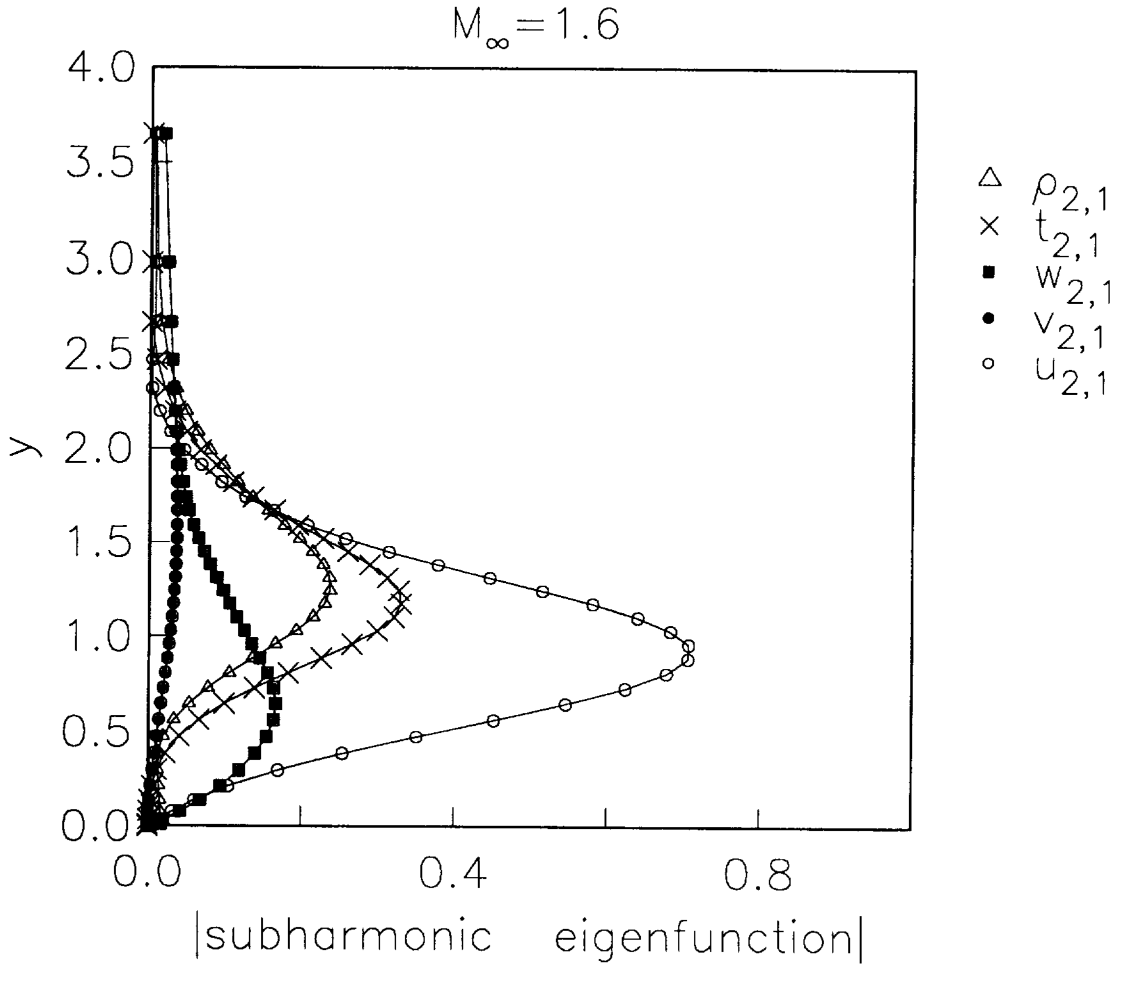

Fig.18: Subharmonic eigenfunction at $M_\infty = 1.6$. The parameters are $\alpha = 0.24$, $\theta = 0^\circ$, $\beta_2 = 0.4$, $T_\infty = 520^0 R$, $Re = 1675$, and $A = 1.5\%$.

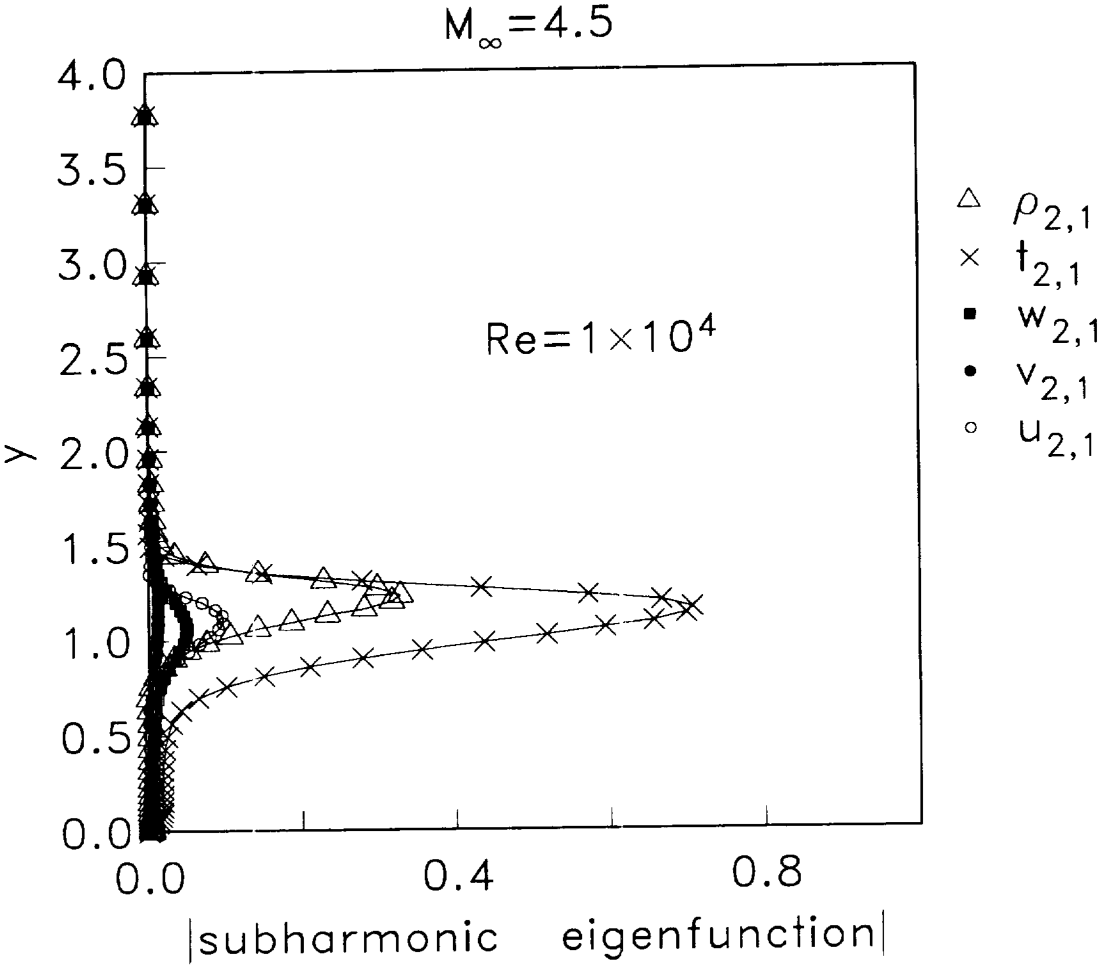

Fig.19: Subharmonic eigenfunction at $M_\infty = 4.5$. The parameters are $\alpha = 2.52$, $\theta = 0^\circ$, $\beta_2 = 2.1$, $T_\infty = 110^\circ R$, $Re = 10000$, and $A = 6\%$.

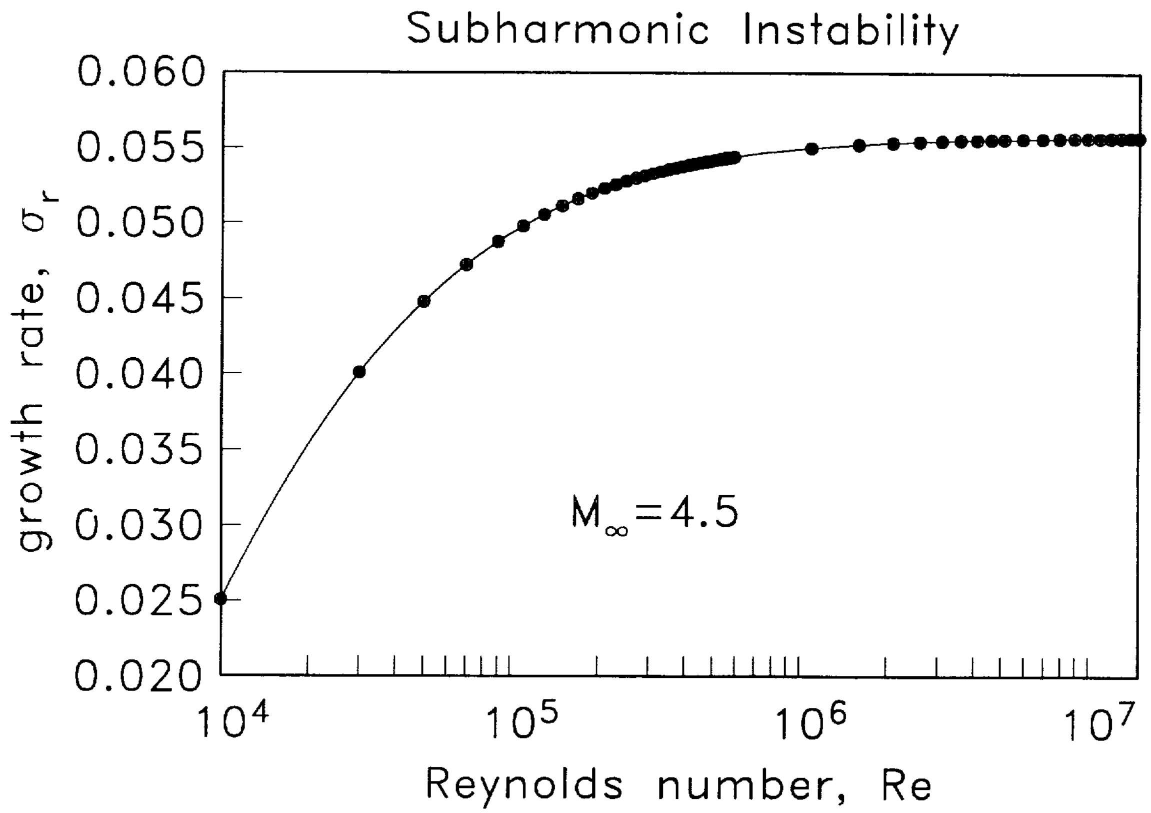

Fig.20: Subharmonic growth rate as a function of the Reynolds number.

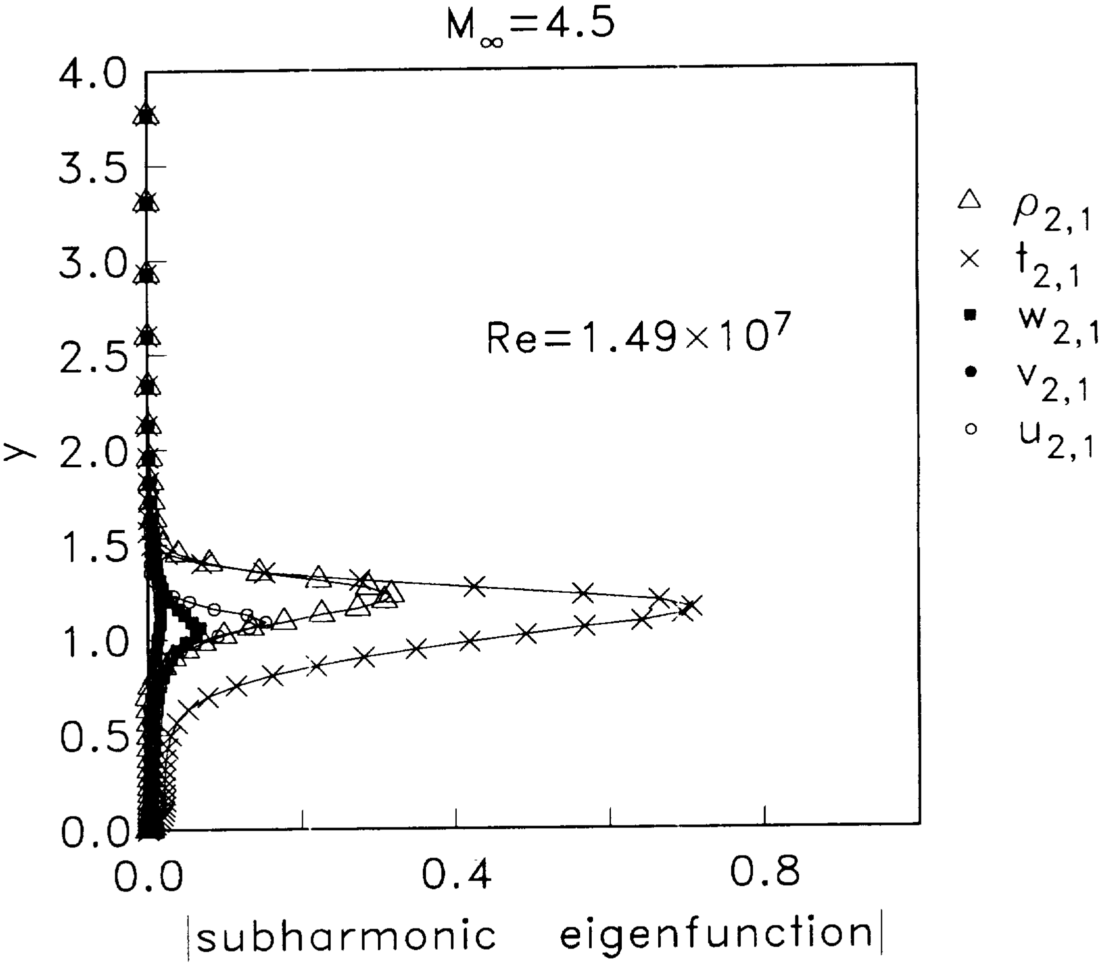

Fig.21: Subharmonic eigenfunction at $Re = 1.49 \times 10^7$.

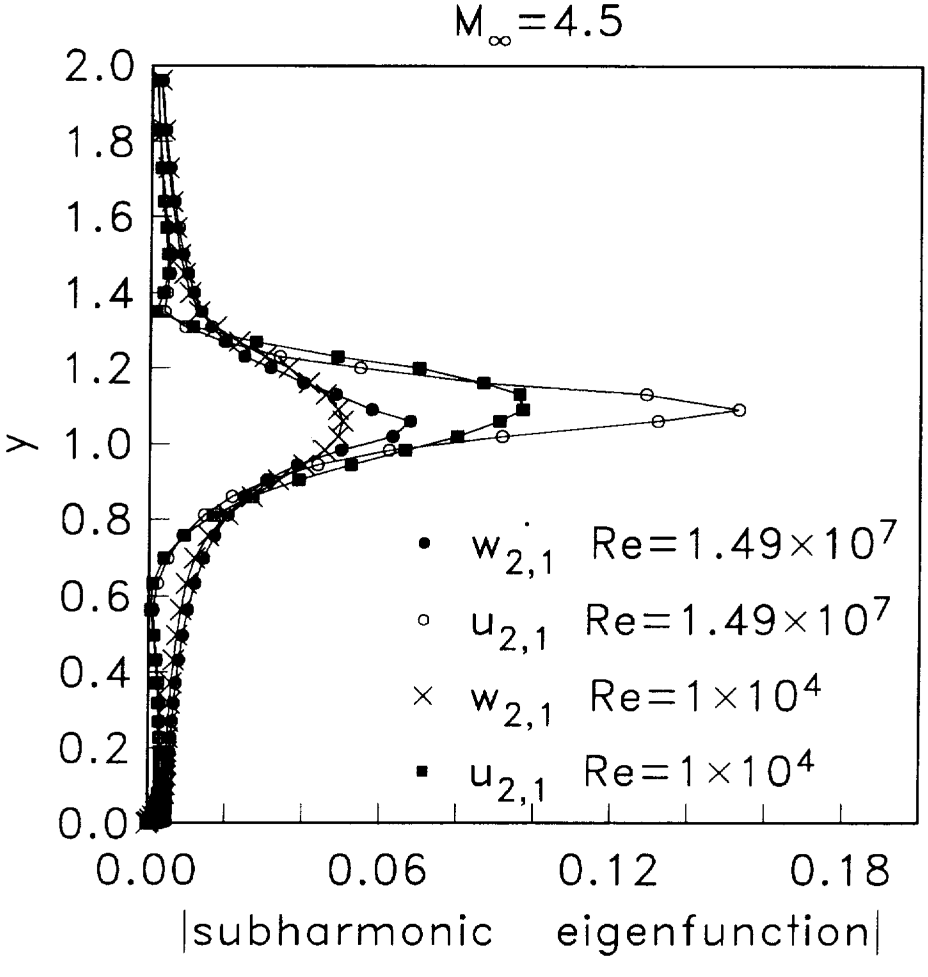

Fig.22: Comparison of the velocity eigenfunctions $w_{2,1}$ and $u_{2,1}$ at $Re = 1 \times 10^4$ and at $Re = 1.49 \times 10^7$.

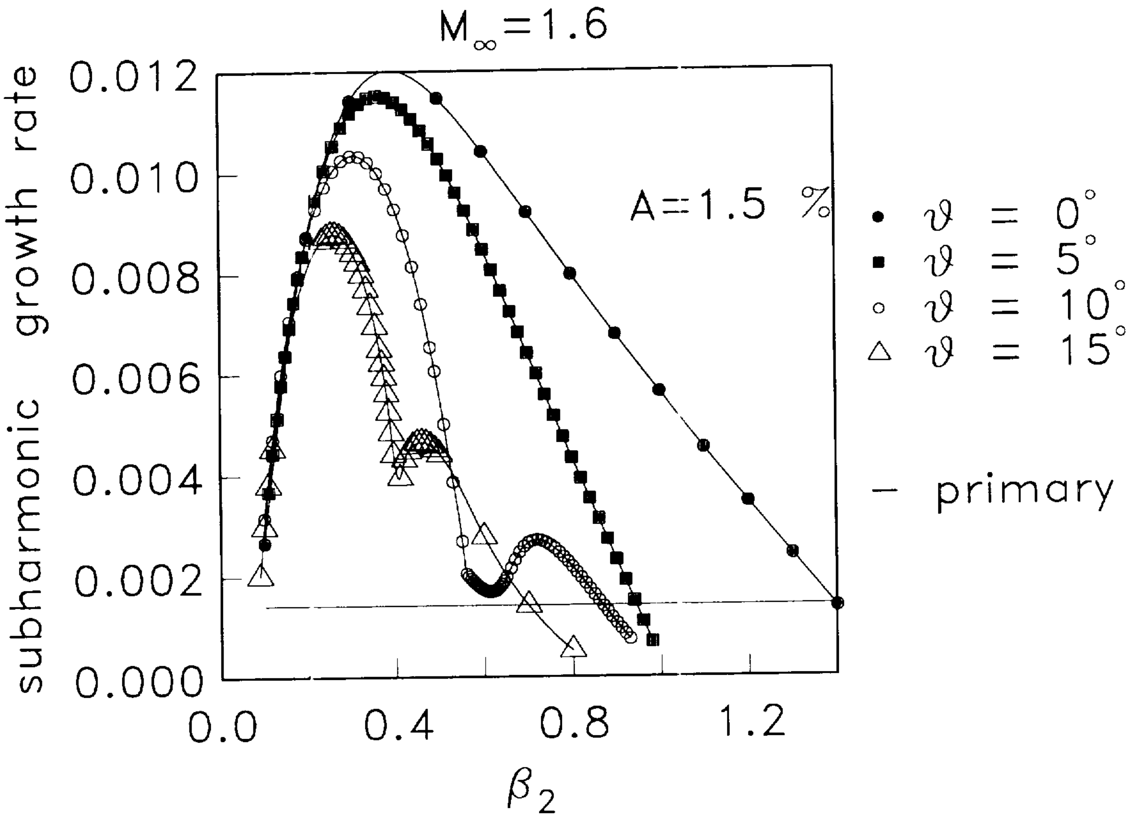

Fig.23: Subharmonic instabilities at $M_\infty = 1.6$ for various θ. —— primary growth rate at $\theta = 45^0$.

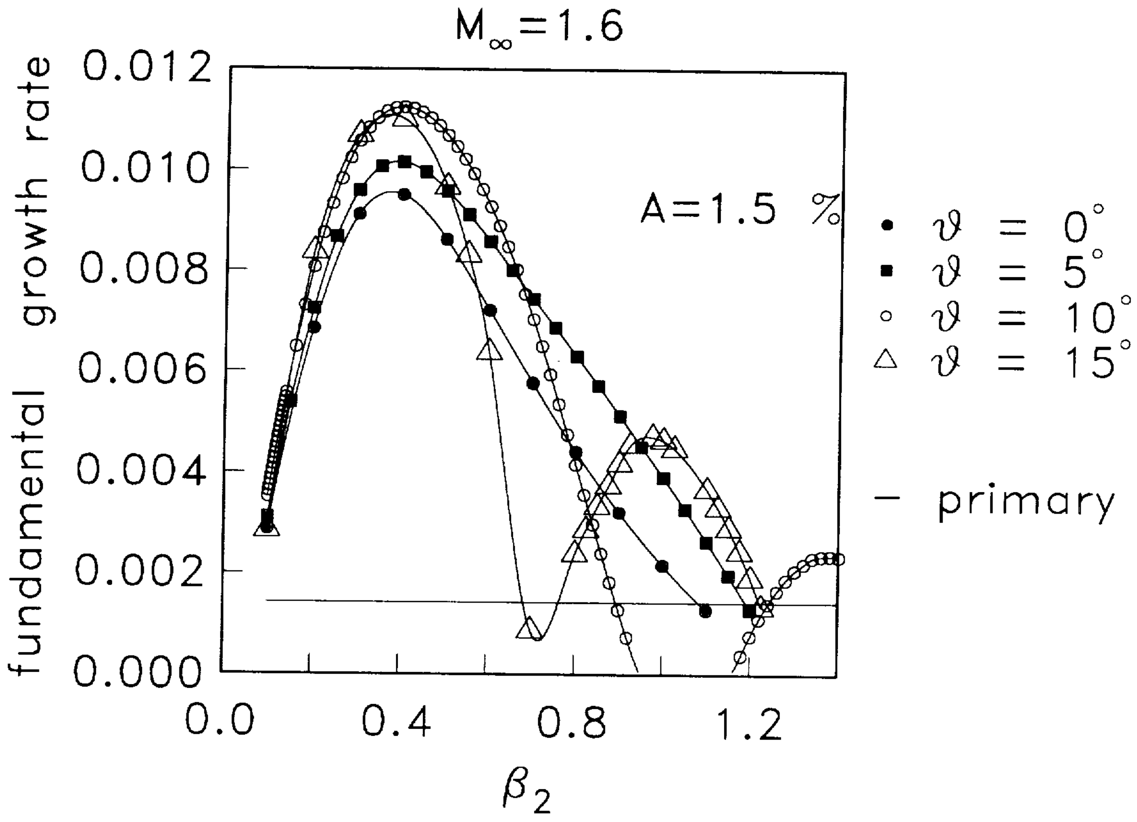

Fig.24: Fundamental instabilities at $M_\infty = 1.6$ for various θ. —— primary growth rate at $\theta = 45^0$.

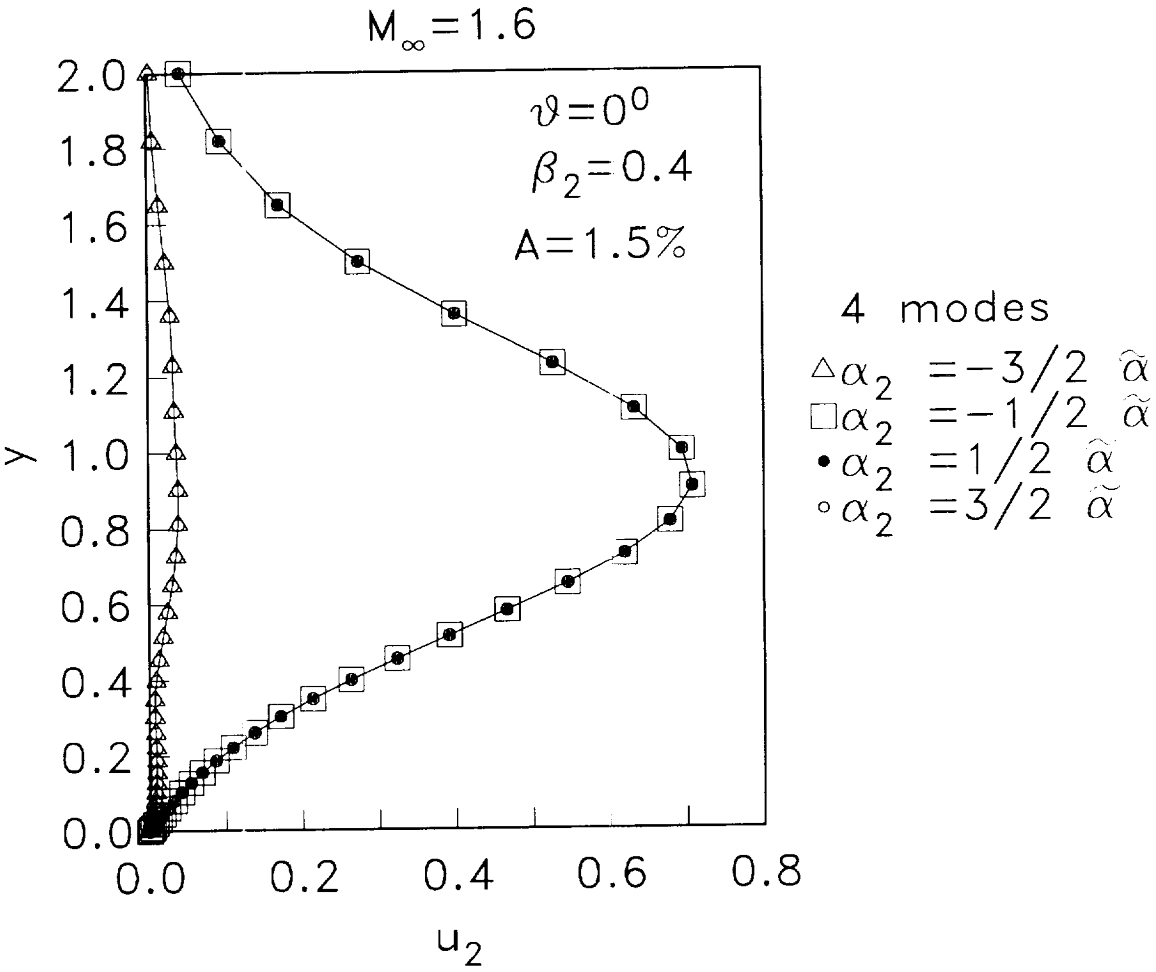

Fig.25: Normalized streamwise velocity components of the subharmonic instability modes at $M_\infty = 1.6$, $\alpha = 0.24$, $\theta = 0^0$, $\beta_2 = 0.4$, $T_\infty = 520^0R$, $Re = 1675$, and $A = 1.5\%$.

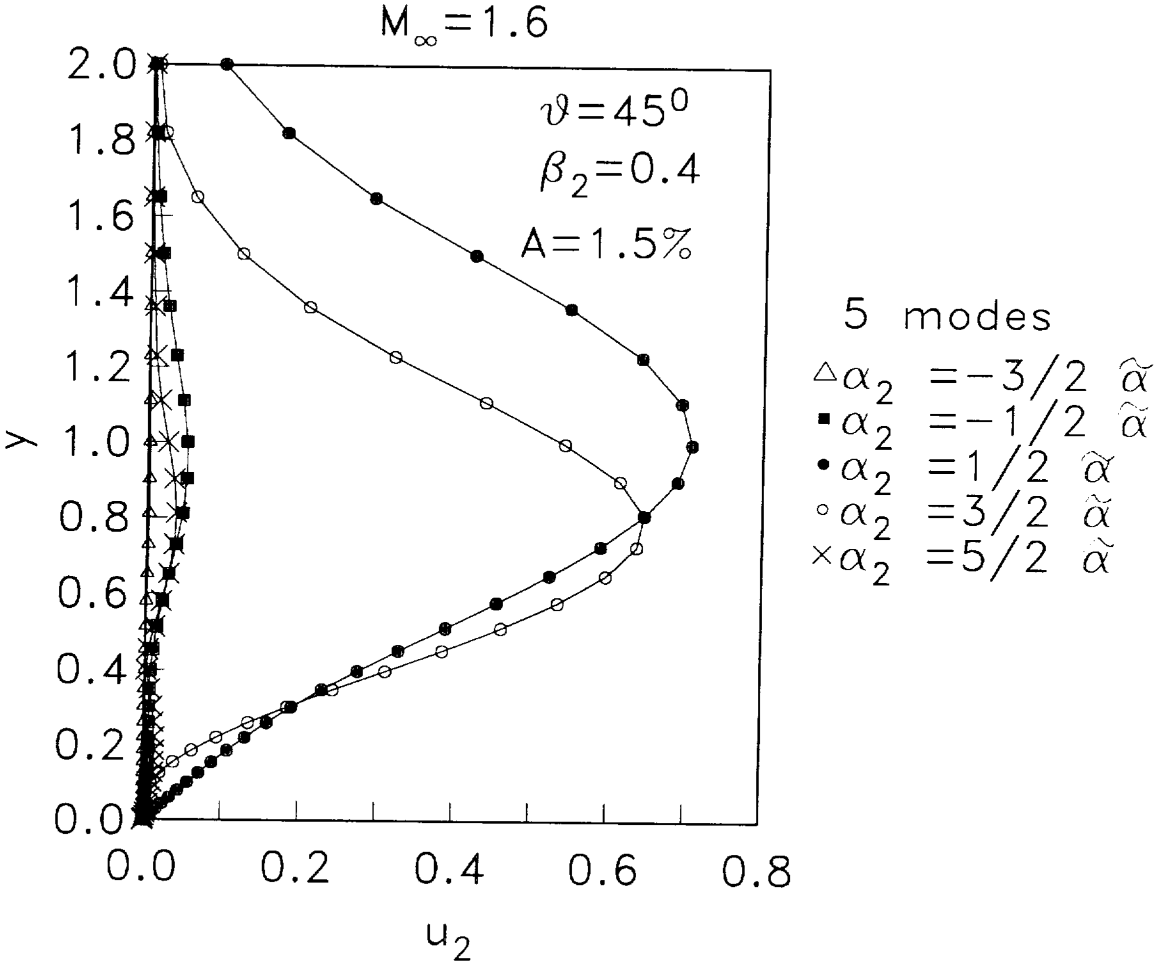

Fig.26: Normalized streamwise velocity components of the subharmonic instability modes at $M_\infty = 1.6$, $\alpha = 0.24$, $\theta = 45^0$, $\beta_2 = 0.4$, $T_\infty = 520^0R$, $Re = 1675$, and $A = 1.5\%$.

NASA
National Aeronautics and Space Administration

Report Documentation Page

1. Report No. NASA CR-182091 ICASE Report No. 90-58	2. Government Accession No.	3. Recipient's Catalog No.

4. Title and Subtitle

SECONDARY INSTABILITIES IN COMPRESSIBLE BOUNDARY LAYERS

5. Report Date

September 1990

6. Performing Organization Code

7. Author(s)

Lian Ng
Gordon Erlebacher

8. Performing Organization Report No.

90-58

10. Work Unit No.

505-90-21-01

9. Performing Organization Name and Address

Institute for Computer Applications in Science
and Engineering
Mail Stop 132C, NASA Langley Research Center
Hampton, VA 23665-5225

11. Contract or Grant No.

NAS1-18605

13. Type of Report and Period Covered

Contractor Report

12. Sponsoring Agency Name and Address

National Aeronautics and Space Administration
Langley Research Center
Hampton, VA 23665-5225

14. Sponsoring Agency Code

15. Supplementary Notes

Langley Technical Monitor:
Richard W. Barnwell

Submitted to Physics of Fluids

Final Report

16. Abstract

This paper examines secondary instabilities in compressible boundary layers at Mach numbers $M_\infty = 0, 0.8, 1.6$, and 4.5. We find that there is a broad-band of highly unstable 3-d secondary disturbances whose growth rates increase with increasing primary wave amplitude. At $M_\infty \leq 1.6$, fundamental resonance dominates at relatively high (2-d) primary disturbance amplitude, while subharmonic resonance is characterized by a low (2-d) primary amplitude. At $M_\infty = 4.5$, the subharmonic instability which arises from the second mode disturbance is the strongest type of secondary instability.

The influence of the inclination, θ, of the primary wave with respect to the mean flow direction on secondary instability is investigated at $M_\infty = 1.6$ for small to moderate values of θ. It is found that the strongest fundamental instability occurs when the primary wave is inclined at 10° to the mean flow direction, although a 2-d primary mode yields the most amplified subharmonic. The subharmonic instability at a high value of θ (namely, $\theta = 45^{\circ}$) is also discussed.

Finally, a subset of the secondary instability results are compared against direct numerical simulations.

17. Key Words (Suggested by Author(s)) transition, compressible boundary layer, secondary instability	18. Distribution Statement 02 - Aerodynamics Unclassified - Unlimited

19. Security Classif. (of this report) Unclassified	20. Security Classif. (of this page) Unclassified	21. No. of pages 52	22. Price A04

NASA FORM 1626 OCT 86

NASA-Langley, 1990